Article

Structure

Structural and Functional Characterization of Ubiquitin Variant Inhibitors of USP15

Graphical Abstract

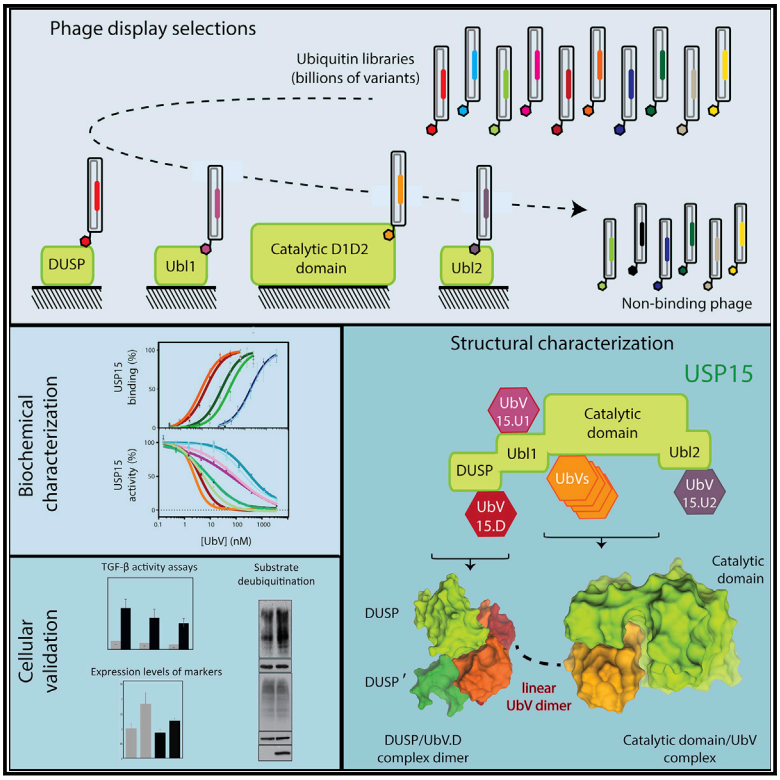

Highlights

- Tight and selective UbVs target USP15 catalytic and adaptor domains
- UbV inhibitors lock the USP15 active site in an inactive conformation
- A strand-swapped UbV dimer binds two DUSP domains simultaneously
- Linear UbV dimers are potent and specific USP15 inhibitors in cells

Authors

Joan Teyra, Alex U. Singer, Frank W. Schmitges, ..., Martin Lenter, Guido Boehmelt, Sachdev S. Sidhu

Correspondence

sachdev.sidhu@utoronto.ca

In Brief

Teyra et al. developed ubiquitin variants (UbVs) that targeted distinct domains of the deubiquitinase USP15 and revealed alternative inhibition and dimerization strategies. Linear UbV dimers exhibited improved potency and specificity of USP15 inhibition. UbVs can be used to study the catalytic mechanism and biological functions of USP15.

Teyra et al., 2019, Structure 27, 590–605
April 2, 2019
https://doi.org/10.1016/j.str.2019.01.002

CellPress

CellPress

Structure
Article

Structural and Functional Characterization of Ubiquitin Variant Inhibitors of USP15

Joan Teyra,[1] Alex U. Singer,[1] Frank W. Schmitges,[1] Patrick Jaynes,[2] Sarah Kit Leng Lui,[2] Maria J. Polyak,[3,4] Nassima Fodil,[3,4] Jonathan R. Krieger,[5] Jiefei Tong,[6] Carsten Schwerdtfeger,[7] Bradley B. Brasher,[7] Derek F.J. Ceccarelli,[8] Jason Moffat,[1,9] Frank Sicheri,[8,9] Michael F. Moran,[5,6,9] Philippe Gros,[3] Pieter J.A. Eichhorn,[2,10,13] Martin Lenter,[11] Guido Boehmelt,[12] and Sachdev S. Sidhu[1,9,14,*]

[1]The Donnelly Centre, University of Toronto, Toronto, ON M5S 3E1, Canada
[2]Cancer Science Institute of Singapore, National University of Singapore, Singapore, Singapore
[3]Department of Biochemistry, McGill University, Montreal, QC, Canada
[4]Corbin Therapeutics, Montreal, QC, Canada
[5]SPARC BioCentre, Hospital for Sick Children, Toronto, ON M5G 0A4, Canada
[6]Cell Biology Program, The Hospital for Sick Children, 686 Bay Street, Toronto, ON M5G 0A4, Canada
[7]Boston Biochem, a Bio-Techne Brand, 840 Memorial Drive, Cambridge, MA 02139, USA
[8]Lunenfeld-Tanenbaum Research Institute, Mount Sinai Hospital, Toronto, ON M5G 1X5, Canada
[9]Department of Molecular Genetics, University of Toronto, Toronto, ON M5S 1A8, Canada
[10]Department of Pharmacology, Yong Loo Lin School of Medicine, National University of Singapore, Singapore, Singapore
[11]Boehringer Ingelheim Pharma GmbH & Co KG, Biberach, Germany
[12]Boehringer Ingelheim RCV GmbH & Co KG, Vienna, Austria
[13]Present address: School of Pharmacy and Biomedical Sciences, Curtin University, Perth 6102, Australia
[14]Lead Contact
*Correspondence: sachdev.sidhu@utoronto.ca
https://doi.org/10.1016/j.str.2019.01.002

SUMMARY

The multi-domain deubiquitinase USP15 regulates diverse eukaryotic processes and has been implicated in numerous diseases. We developed ubiquitin variants (UbVs) that targeted either the catalytic domain or each of three adaptor domains in USP15, including the N-terminal DUSP domain. We also designed a linear dimer (diUbV), which targeted the DUSP and catalytic domains, and exhibited enhanced specificity and more potent inhibition of catalytic activity than either UbV alone. In cells, the UbVs inhibited the deubiquitination of two USP15 substrates, SMURF2 and TRIM25, and the diUbV inhibited the effects of USP15 on the transforming growth factor β pathway. Structural analyses revealed that three distinct UbVs bound to the catalytic domain and locked the active site in a closed, inactive conformation, and one UbV formed an unusual strand-swapped dimer and bound two DUSP domains simultaneously. These inhibitors will enable the study of USP15 function in oncology, neurology, immunology, and inflammation.

INTRODUCTION

Ubiquitination is a reversible post-translational modification that targets proteins for degradation and regulates their activity and localization (Grabbe et al., 2011). Monoubiquitin or polyubiquitin chains are appended to substrates by E1/E2/E3 ligases, and may subsequently be removed by deubiquitinases (DUBs) to reverse signals or stabilize proteins (Clague et al., 2013). As knowledge has accumulated regarding the structure, function, and biology of DUBs (Clague et al., 2012; Heideker and Wertz, 2015), it has become apparent that each DUB plays a distinct role in the regulation of different components in cell biology and signaling (Darling et al., 2017; Kumari et al., 2017; Lim et al., 2016; Pinto-Fernandez and Kessler, 2016).

USP15 is a widely expressed DUB that regulates multiple diverse cellular processes (Fielding et al., 2018). Copy-number gains of the *USP15* gene have been reported in glioblastoma, and breast and ovarian cancers (Eichhorn et al., 2012), whereas copy-number losses have been identified in pancreatic cancer (Srihari and Ragan, 2013). Proposed substrates for USP15 include numerous cancer-associated proteins in various signaling pathways, such as the human papilloma virus E6 oncoprotein (Vos et al., 2009), adenomatosis polyposis coli tumor suppressor (Huang et al., 2009), nuclear factor of κ light polypeptide gene enhancer in B cells inhibitor α (Schweitzer et al., 2007), the transforming growth factor β (TGF-β) receptor (TβR) (Eichhorn et al., 2012) and its receptor-regulated SMAD effectors (Inui et al., 2011), p53 (Liu et al., 2017), human homolog of mouse double minute 2 (Zou et al., 2014), and the ubiquitin (Ub) E3 ligase BRCA1-associated protein associated with the Ras-MAPK signaling cascade (Hayes et al., 2012). Recently, USP15 has also been shown to play an important regulatory role in the immune system, including modulation of the inflammatory response, and *Usp15*$^{-/-}$ mice display altered activity of leukocytes in models of infectious and inflammatory diseases (Torre et al., 2017).

These diverse substrates and biological functions for USP15 suggest that its cellular activity must be tightly regulated and directed. Although USP15 predominantly localizes to the

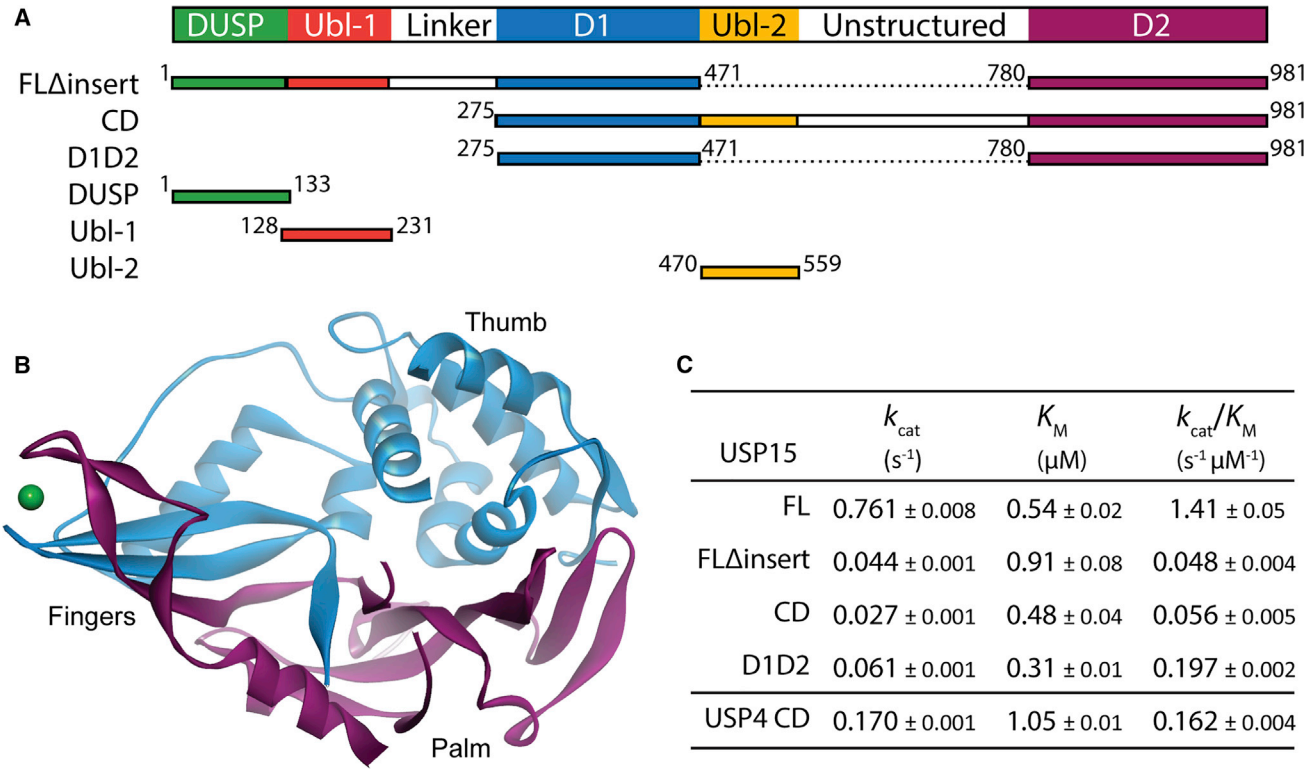

C

USP15	k_{cat} (s^{-1})	K_M (μM)	k_{cat}/K_M (s^{-1} $μM^{-1}$)
FL	0.761 ± 0.008	0.54 ± 0.02	1.41 ± 0.05
FLΔinsert	0.044 ± 0.001	0.91 ± 0.08	0.048 ± 0.004
CD	0.027 ± 0.001	0.48 ± 0.04	0.056 ± 0.005
D1D2	0.061 ± 0.001	0.31 ± 0.01	0.197 ± 0.002
USP4 CD	0.170 ± 0.001	1.05 ± 0.01	0.162 ± 0.004

Figure 1. Domain Architecture and Catalytic Activity of USP15 and USP4

(A) Schematic representation of human USP15 with demarcation of structured domains. The USP15 protein fragments and nomenclature used in this study are shown below the schematic with the residue numbers of the boundaries indicated. Dots indicate deletions within a fragment.

(B) The structure of the D1D2 domain of USP15 (PDB: 6GHA) is shown as a ribbon with D1 and D2 colored blue or purple, respectively, and the chelated Zn^{2+} ion is shown as a green sphere.

(C) Catalytic rate constants for the hydrolysis of Ub-AMC by USP15 FL, USP15 fragments, and USP4 CD. Values were determined from Michaelis-Menten plots and errors represent the SD of three independent experiments.

See also Figure S1.

cytoplasm (Urbé et al., 2012), it performs specific functions in the nucleus (Long et al., 2014) and mitochondria (Cornelissen et al., 2014). Mechanisms to control USP15 activity within cells are suggested by evidence that USP15 is alternatively spliced (Kotani et al., 2017) and can be ubiquitinated and phosphorylated (Hayes et al., 2012; Olsen et al., 2010; Wagner et al., 2011). Despite these insights, it remains unclear how the cell maintains control over the diverse functions of USP15.

USP15 belongs to the Ub-specific protease (USP) family, the largest DUB structural family containing ~56 members in humans, and shares the same domain architecture and high sequence similarity with two homologs, USP4 (57% similarity) and USP11 (43% similarity) (Chou et al., 2017). In addition to the catalytic domain, USP15 contains a DUSP domain (domain present in Ub-specific proteases), which has no described function and is found exclusively in USP proteins (Clague et al., 2013), and two Ub-like (Ubl) domains, which share the conserved β-grasp fold of Ub (Burroughs et al., 2007). The DUSP domain and the first Ubl domain (Ubl-1) precede the USP15 catalytic domain, which is composed of two lobes (D1 and D2) separated by a large insert (CD-insert) that contains the second Ubl domain (Ubl-2) and a predicted unstructured region (Figure 1A).

USP15 is expected to function similarly to the extensively studied USP4. The structures of the USP15 and USP4 D1D2 domains resemble the papain-like fold of other USP catalytic domains, consisting of an extended structure comprising three regions—fingers, thumb, and palm—that together form the Ub-binding pocket (Figure 1B) (Komander et al., 2009; Ward et al., 2018). The catalytic cleft, which accommodates the C-terminal tail of substrate Ub, is located between the palm and thumb, whereas two Cys-X-X-Cys motifs, which coordinate a zinc ion and stabilize a zinc-finger ribbon structure, are located at the tips of the fingers (Tencer et al., 2016). The *in vitro* activity of DUBs is often low, hinting at activation mechanisms imposed by cellular context. Notably, the apo structures of USP15 and USP4 catalytic domains show that the substrate-binding sites are occluded by the zinc-finger ribbons in a "closed-hand" conformation, suggesting that conformational changes are required for enzyme activity (Clerici et al., 2014; Ward et al., 2018).

Although USP15 and other DUBs have attracted attention as potential therapeutic targets, the development of selective DUB inhibitors has been limited by insufficient understanding of DUB biology, difficulties in establishing robust biochemical assays for compound screening, limitations in cellular and *in vivo*

models to assess DUB activity and inhibition, and the non-specific nature of most available small-molecule inhibitors (Harrigan et al., 2018). Thus, alternative methods are needed to probe the mechanisms and consequences of DUB inhibition, and we have established an approach that uses engineered Ub variants (UbVs) as modulators of DUBs, E3 ligases, and adaptor proteins within the Ub proteasome system (UPS). The large, solvent-accessible surface of Ub that mediates low-affinity interactions with a variety of proteins is amenable to engineering, and phage-displayed combinatorial libraries that diversify this surface have yielded tight and selective UbVs to target many components of the UPS (Gorelik et al., 2016).

Here we generated selective UbVs for each individual USP15 domain, including the catalytic domain, the DUSP domain, and the two Ubl domains, and used biochemical and structural studies to characterize USP15/UbV complexes. We also developed linear UbV dimers composed of UbVs targeting the DUSP and catalytic domains, which further improved the potency and specificity of USP15 inhibition. Despite exhibiting some interaction with the close homolog USP4 (Vlasschaert et al., 2015), optimized UbVs bound specifically to USP15 in cells and inhibited its deubiquitinating activity toward its substrates SMURF2 and TRIM25. Moreover, a UbV dimer inhibited the effects of USP15 in the TGF-β pathway. Taken together, our work demonstrates the versatility of the UbV technology and provides powerful inhibitors to elucidate the intricacies of USP15 function in both normal and disease biology.

RESULTS

Minimization of the USP15 Catalytic Domain

The USP15 and USP4 catalytic domains adopt occluded conformations, and interactions with DUSP-Ubl-1 and the CD-insert significantly affect activation (Ward et al., 2018; Clerici et al., 2014). To gain insight into the structure and function of USP15, we tested the catalytic activities of commercial full-length USP15 (USP15 FL) produced in insect cells (Boston Biochem) and USP15 protein fragments expressed recombinantly in *Escherichia coli* (Figure 1A). We purified the following USP15 protein fragments: deletion of CD-insert (FLΔinsert), deletion of residues preceding the catalytic domain (CD), and deletion of CD-insert and residues preceding the catalytic domain (D1D2). Catalytic rate constants were determined by measuring catalytic rates over a range of substrate concentrations and fitting the data to the Michaelis-Menten equation (Figures 1C and S1). The slope was determined from the linear phase of product accumulation, which typically occurred 100 s after initiation of the reaction, as described previously (Clerici et al., 2014). The three fragments containing the catalytic domain retained catalytic activity for a minimal fluorogenic substrate, Ub C-terminal 7-amido-4-methylcoumarin (Ub-AMC) (Dang et al., 1998). However, they were less active than USP15 FL and were compromised in turnover (k_{cat}) rather than substrate recognition (K_M). Notably, others have shown that recombinant USP15 FL purified from *E. coli* is less active than USP15 FL purified from insect cells (Clerici et al., 2014; Ward et al., 2018), suggesting that eukaryotic expression might aid folding and modification of USP15 to achieve full catalytic efficiency (Jarvis, 2009). We also purified the USP4 catalytic domain (USP4 CD) and found that it exhibited significant catalytic activity comparable with that of USP15 CD (Figures 1C and S1). Thus, we were able to purify recombinant protein fragments of USP15 and USP4 that exhibited catalytic activity and could be used to generate and characterize UbV inhibitors.

Generation and Optimization of UbV Binders for USP15

We previously designed a UbV library (library 2) in which 29 positions on the Ub surface were subjected to a diversification strategy that favored the wild-type sequence (soft randomization) and four C-terminal positions were diversified in a completely random manner (hard randomization) (Ernst et al., 2013). Library 2 has been used to develop tight and specific UbV binders for a variety of UPS components, including DUBs (Ernst et al., 2013; Zhang et al., 2017) and E3 ligases (Gabrielsen et al., 2017; Gorelik et al., 2016; Zhang et al., 2016b). We analyzed the sequences of UbVs characterized in these previous studies to aid the design of a new library 4 (Figure 2A and Table S1). In library 4, we targeted eight positions that formed a contiguous patch on the surface and were mutated frequently in previous UbVs (Lys^6, Leu^8, Thr^9, Thr^{12}, Thr^{66}, His^{68}, Val^{70}, Leu^{71}), and also the last two residues (Gly^{75} and Gly^{76}). In our previous studies of SCF E3 ligases (Gorelik et al., 2016), we observed that the β1-β2 loop of UbVs could tolerate insertions that enhanced affinity and specificity, so we allowed for the insertion of one, two, or three residues between positions Leu^8 and Thr^9. Thus, the library 4 design involved hard randomization of 10–13 positions, and the constructed library contained 2.5×10^{10} unique members.

We pooled libraries 2 and 4 and selected for UbVs that bound to various USP15 protein fragments. Following selections, we used phage ELISAs to identify clones that bound specifically to particular proteins and used DNA sequencing to decode the sequences of the UbVs (data not shown). Based on these analyses, we focused on one unique binder each for the DUSP domain (UbV.15.D), the Ubl-1 domain (UbV.15.U1), and the Ubl-2 domain (UbV.15.U2), and two unique binders for D1D2 (UbV.15.1 and 2) (Figure 2B). UbVs 15.D, 15.U1, and 15.U2 contained inserts in the β1-β2 loop and were thus derived from library 4, whereas UbVs 15.1 and 15.2 did not contain inserts in the β1-β2 loop and were derived from library 2. UbV proteins were purified and tested for binding to various USP15 and USP4 protein fragments (Figures 2B, S2, and S3). Wild-type Ub (Ub.wt) did not exhibit appreciable binding to any of the protein fragments. As expected, UbV.15.D bound to USP15 DUSP and FLΔinsert with high affinity, but it did not bind to USP15 D1D2 or USP4 DUSP-Ubl-1. Also as expected, UbV.15.U1 bound to USP15 Ubl-1 and FLΔinsert with similar affinities and did not bind to USP15 D1D2, but it also bound to USP4 DUSP-Ubl-1 with 3-fold lower affinity, suggesting that it recognized the Ubl-1 domains of USP15 and USP4, which share 67% sequence identity. UbV.15.U2 exhibited high specificity as it only bound tightly to USP15 Ubl-2. Finally, UbVs 15.1 and 15.2 bound to USP15 D1D2 and FLΔinsert, indicating that these UbVs recognized the catalytic D1D2 domain. Taken together, these results show that we were able to develop specific UbVs that bound to each of the four known structured domains within USP15 (DUSP, Ubl-1, Ubl-2, and D1D2).

As we aimed to develop inhibitors of USP15 catalytic activity, we focused further optimization efforts on UbVs that bound to

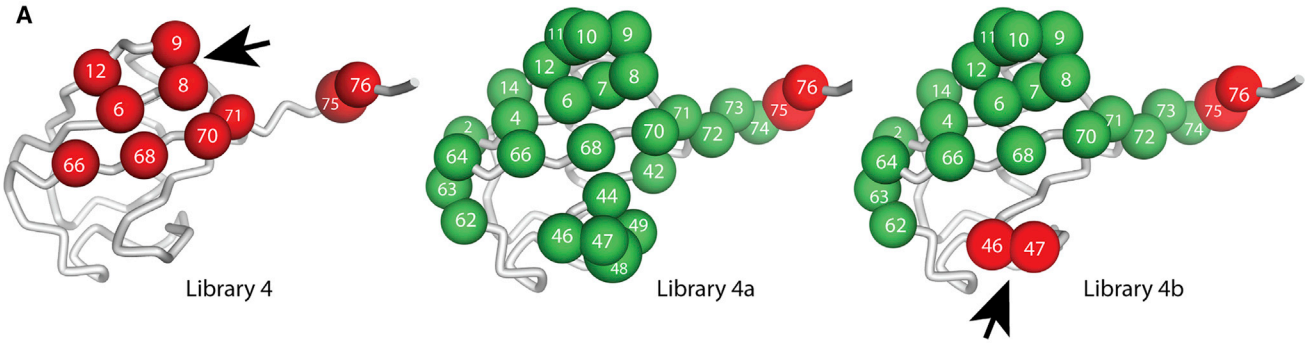

B

	Region 1														Region 2																Region 3																EC$_{50}$ (nM)			
	2	4	6	7	8	a	b	c	9	10	11	12	14		42	44	46	a	b	c	d	e	f	g	h	47	48	49		62	63	64	66	68	70	71	72	73	74	75	76	77	78		USP15	USP15	USP15	USP4
Ub.wt	Q	F	K	T	L	.	.	.	T	G	K	T	T		R	I	A	.	.	.	.	.	.	.	.	G	K	Q		Q	K	E	T	H	V	L	R	L	R	G	G	G	G		FLΔinsert	D1D2	Domains	DUSP-Ubl-1
15.D	-	-	S	-	A	W	F	.	C	-	-	L	-		-	-	-	-	-	-	-	-	-	-	-	-	-	-		-	-	G	Q	H	R	-	-	-	P	T	.	.		3.7	>1000	2.3 [a]	>1000
15.U1	-	-	G	-	V	M	.	.	L	-	-	S	-		-	-	-	-	-	-	-	-	-	-	-	-	-	-		-	-	W	L	R	M	-	-	-	A	T	.	.		77	>1000	57 [b]	211
15.U2	-	-	G	-	I	L	K	Y	R	-	-	F	-		-	-	-	-	-	-	-	-	-	-	-	-	-	N		-	-	F	F	L	V	-	-	-	A	P	.	.		>1000	>1000	41 [c]	>1000
15.1	L	-	-	-	A	.	.	.	P	-	-	I	N		K	T	-	.	.	.	.	.	.	.	.	S	-	-		-	-	H	Y	-	-	-	I	-	-	-	L	N	W		210	58	-	-
15.2	-	-	-	-	-	-	-	-	.	.	A	S	-	F	S		-	-	-	-	-	-	-	-	-	-	-	-	-		-	-	Y	-	-	L	-	-	-	-	-	-	-		190	78	-	-
15.1a	L	-	-	-	-	-	-	-	S	-	-	F	S		-	-	-	G	K	R	L	S	F	Y	.	R	-	-		-	-	H	-	Q	L	V	I	S	L	Y	.	.	.		4.8	6.6	-	-
15.1b	V	-	-	-	H	.	.	.	-	-	-	F	P		-	-	-	G	K	Q	G	L	G	F	Y	R	-	L		-	-	-	-	-	-	-	-	-	-	-	-	-	-		19	13	-	-
15.1c	W	-	-	S	A	.	.	.	A	-	-	L	P		-	-	-	G	K	Q	M	L	G	F	W	R	R	E		-	-	-	-	-	-	-	-	-	-	-	-	-	-		8.2	9.2	-	-
15.1d	-	-	-	-	P	.	.	.	-	-	-	F	S		-	-	R	Q	T	W	A	.	.	.	.	S	-	-		-	-	-	-	-	-	-	-	-	-	-	-	-	-		0.9	1.9	-	-
15.1e	-	-	-	-	-	-	-	-	-	-	-	I	S		-	-	R	G	F	H	W	K	P	.	.	L	-	-		-	-	-	-	-	-	-	-	-	-	-	-	-	-		1.5	3.0	-	-

Figure 2. UbVs Selected for Binding to USP15 Domains

(A) Designs of phage-displayed UbV libraries 4 (left), 4a (center), and 4b (right) mapped onto the Ub.wt structure (PDB: 1UBQ). The Ub.wt backbone is shown as a gray tube, positions that were diversified are shown as spheres, and loop insertion points are shown by arrows. The spheres are colored red or green for positions that were hard or soft randomized, respectively. Loop insertions were hard randomized with one, two, or three codons inserted between positions 8 and 9 in library 4, and four, six, or eight codons inserted between positions 47 and 48 in library 4b.

(B) Sequence alignment of Ub.wt and UbVs, and EC_{50} values for binding to fragments of USP15 and USP4. The alignment shows only those positions that were diversified in the UbV libraries, and dashes or dots indicate conservation or insertion relative to Ub.wt, respectively. EC_{50} values were determined by ELISA with UbV proteins binding to immobilized USP proteins. In the column "USP15 domains," the following domains are represented: a = DUSP, b = Ubl-1, c = Ubl-2. Dashes indicate that assays were not performed.

See also Figures S2 and S3.

USP15 fragments containing the catalytic domain, reasoning that these would be most likely to act as inhibitors. We chose UbV.15.1 rather than UbV.15.2 for further optimization, because its sequence was most divergent from Ub.wt and we reasoned that it would be less likely to interact with other proteins that interact with Ub.wt. To improve the affinity of UbV.15.1 for USP15, we constructed library 4a, in which 26 positions that are frequently buried at the interface between Ub.wt and the Ub-binding sites of USPs were subjected to soft randomization that favored the UbV.15.1 sequence, and the two C-terminal positions were hard randomized (Figure 2A). Binding selections and subsequent sequencing and binding analyses yielded three UbVs (15.1a, 15.1b, and 15.1c) that bound to FLΔinsert and D1D2 much more tightly than did UbV.15.1 (Figure 2B). In addition to designed substitutions, the three UbVs contained a homologous insertion between positions 46 and 47 of the β3-β4 loop, which was not included in the library design. Notably, the first three residues of these insertions also exhibited homology to residues 47–49 of Ub.wt, suggesting that they may have arisen through a DNA-duplication event. The fact that insertions arose independently in three distinct UbVs suggested that particular extensions of the β3-β4 loop may enhance affinity for USP15. Thus, we designed library 4b based on the sequence of UbV.15.1, in which 20 residues were soft randomized and the two C-terminal positions were hard randomized. In addition, hard randomized loops of 4, 6, or 8 residues were inserted between positions Ala[46] and Gly[47], which were also hard randomized (Figure 2A). Binding selections and subsequent analyses yielded two UbVs (15.1d and 15.1e) with affinities for D1D2 improved 30- and 20-fold, respectively, relative to UbV.15.1 (Figure 2B). Compared with Ub.wt, the main differences in UbVs 15.1d and 15.1e were β3-β4 loop insertions of four or six residues, respectively, suggesting that extended β3-β4 loops were mainly responsible for the dramatic enhancements in affinity for USP15. Taken together, these results show that UbVs with high affinity for the USP15 catalytic domain can be developed by optimization of the Ub.wt surface and by engineering extensions in the β3-β4 loop.

Assessment of UbV Activity *In Vitro*

To identify competitive inhibitors of USP15, we used an assay with USP15 fragments that measured hydrolysis of Ub-AMC, a substrate that binds directly to the Ub-binding sites of USP catalytic domains (Table 1 and Figure S4) (Dang et al., 1998). As expected, the UbVs that bound to DUSP, Ubl-1, or Ubl-2 domains did not affect Ub-AMC hydrolysis by USP15 FLΔinsert (Figure S4A). In contrast, all of the UbVs that bound to D1D2 and FLΔinsert (Figure 2B) inhibited Ub-AMC hydrolysis by USP15

Table 1. IC_{50} Values for Inhibition of DUB Activity by UbVs

UbV	IC_{50} (nM)[a]												
	USP15	USP15 FLΔinsert	USP15 CD	USP4	USP4 CD	USP11	USP19	USP2	USP7	USP8	USP9x	USP28	UCHL1	UCHL5
15.1	90 ± 20	50 ± 4	150 ± 20	700 ± 20	>1,000	>1,000	>1,000	>1,000	>1,000	>1,000	>1,000	>1,000	>1,000	>1,000
15.2	90 ± 20	50 ± 3	300 ± 50	600 ± 90	>1,000	>1,000	>1,000	>1,000	>1,000	>1,000	>1,000	>1,000	>1,000	>1,000
15.1a	20 ± 2	10.1 ± 0.5	4.9 ± 0.6	90 ± 30	70 ± 7	400 ± 70	400 ± 30	>1,000	>1,000	>1,000	>1,000	>1,000	>1,000	>1,000
15.1b	20 ± 5	30 ± 6	8.5 ± 0.6	200 ± 3	100 ± 20	900 ± 80	>1,000	>1,000	>1,000	>1,000	>1,000	>1,000	>1,000	>1,000
15.1c	50 ± 10	20 ± 4	7.4 ± 0.3	200 ± 20	30 ± 6	>1,000	300 ± 40	>1,000	>1,000	>1,000	>1,000	>1,000	>1,000	>1,000
15.1d	10 ± 2	4.7 ± 0.2	2.3 ± 0.1	40 ± 3	7 ± 3	70 ± 10	40 ± 5	>1,000	>1,000	>1,000	>1,000	>1,000	>1,000	>1,000
15.1e	30 ± 2	5.4 ± 0.1	3.7 ± 0.3	80 ± 6	3 ± 1	60 ± 20	600 ± 100	>1,000	>1,000	>1,000	>1,000	>1,000	>1,000	>1,000
15.1/D	6.6 ± 0.8	10 ± 1	90 ± 20	600 ± 30	>1,000	>1,000	>1,000	>1,000	>1,000	>1,000	>1,000	>1,000	>1,000	>1,000
15.D/1	10 ± 3	5.3 ± 0.4	80 ± 20	600 ± 50	>1,000	>1,000	>1,000	>1,000	>1,000	>1,000	>1,000	>1,000	>1,000	>1,000

All proteins were full length unless otherwise indicated.
Ub-Rh110 substrate was used for all enzymes except USP FLΔinsert, USP CD, and USP4 CD, for which Ub-AMC substrate was used.
[a]The IC_{50} value was defined as the concentration of UbV required to inhibit 50% of the activity of the enzyme for hydrolysis of the substrate. Data are presented as mean ± SD (n = 3).

in a dose-dependent manner (Table 1). Notably, this assay showed improvements in potency for all USP15 fragments in going from the first-generation UbVs 15.1 and 15.2 (IC_{50} ~50–100 nM), to the second-generation UbVs 15.1a, 15.1b, and 15.1c (IC_{50} ~10–30 nM), to the third-generation UbVs 15.1d and 15.1e (IC_{50} ~5–10 nM) (Table 1). Ub-AMC hydrolysis assays also showed that, whereas the first-generation UbVs inhibited USP4 very weakly, the second- and third-generation UbVs inhibited USP4 with potencies that were similar to those for USP15 (Table 1). Taken together, these results confirm that we were successful in developing UbVs that bound to the USP15 catalytic domain and inhibited activity, and although potency could be improved by extension and optimization of the β3-β4 loop, these improvements came with a loss of discrimination against the homolog USP4.

Construction and Characterization of Dimeric UbVs

As an alternative approach to generating potent and specific inhibitors, we took advantage of the UbVs that we had on hand for the various USP15 domains. We reasoned that dimeric UbVs (diUbVs) that linked together two specific USP15 binders recognizing distinct domains may maintain high specificity while achieving higher potency due to avidity effects endowed by simultaneous binding to two sites. We linked UbV.15.1, which bound and inhibited USP15 with modest potency but did not inhibit USP4 (Table 1), and UbV.15.D, which did not inhibit USP15 but bound the USP15 DUSP domain with high affinity (EC_{50} = 2 nM) and did not bind the USP4 DUSP-Ubl-1 fragment (Figure 2B). Fusion proteins in which UbV.15.1 and UbV.15.D were connected by a flexible 16-residue linker (GSGSGSGSGSGSGSGS), with UbV.15.1 at either the N-terminal (diUbV.15.1/D) or C-terminal end (diUbV.15.D/1), inhibited USP15 FLΔinsert activity 5- or 10-fold more potently than UbV.15.1 alone, respectively (Table 1 and Figure S4). Notably, inhibition of USP15 CD was ~10-fold less efficient than inhibition of FL or FLΔinsert, suggesting that optimal inhibition by the diUbVs requires binding to both CD and DUSP. Importantly, the diUbVs were poor inhibitors of USP4, demonstrating that the strategy achieved both potent and specific inhibition of USP15.

Assessment of UbV Specificity

To assess and compare the strength and specificity of interactions in a physiologically relevant context, we transiently expressed various FLAG-tagged UbVs and diUbVs in HEK293T cells and analyzed the amounts of USP15 and USP4 associated with each UbV by performing immunoprecipitation of the UbV followed by mass spectrometry (IP-MS; Figures 3A and 3B). Consistent with *in vitro* affinity and specificity profiles showing higher potency but lower specificity (Table 1), the second-generation UbVs (15.1a, 15.1b, and 15.1c) precipitated more USP15 but also more USP4 than did the first generation UbVs (15.1 and 15.2). Somewhat unexpectedly, the third-generation UbVs (15.1d and 15.1e) were less efficient than the second-generation UbVs for co-precipitation of USP15, and also precipitated more USP4 and additional USP proteins (USP19, UCHL2 and UCHL3; Figure 3C). In contrast, both diUbVs were much more efficient at co-precipitating USP15 than any single UbV, with diUbV.15.1/D showing >100-fold better efficiency than either of the UbVs

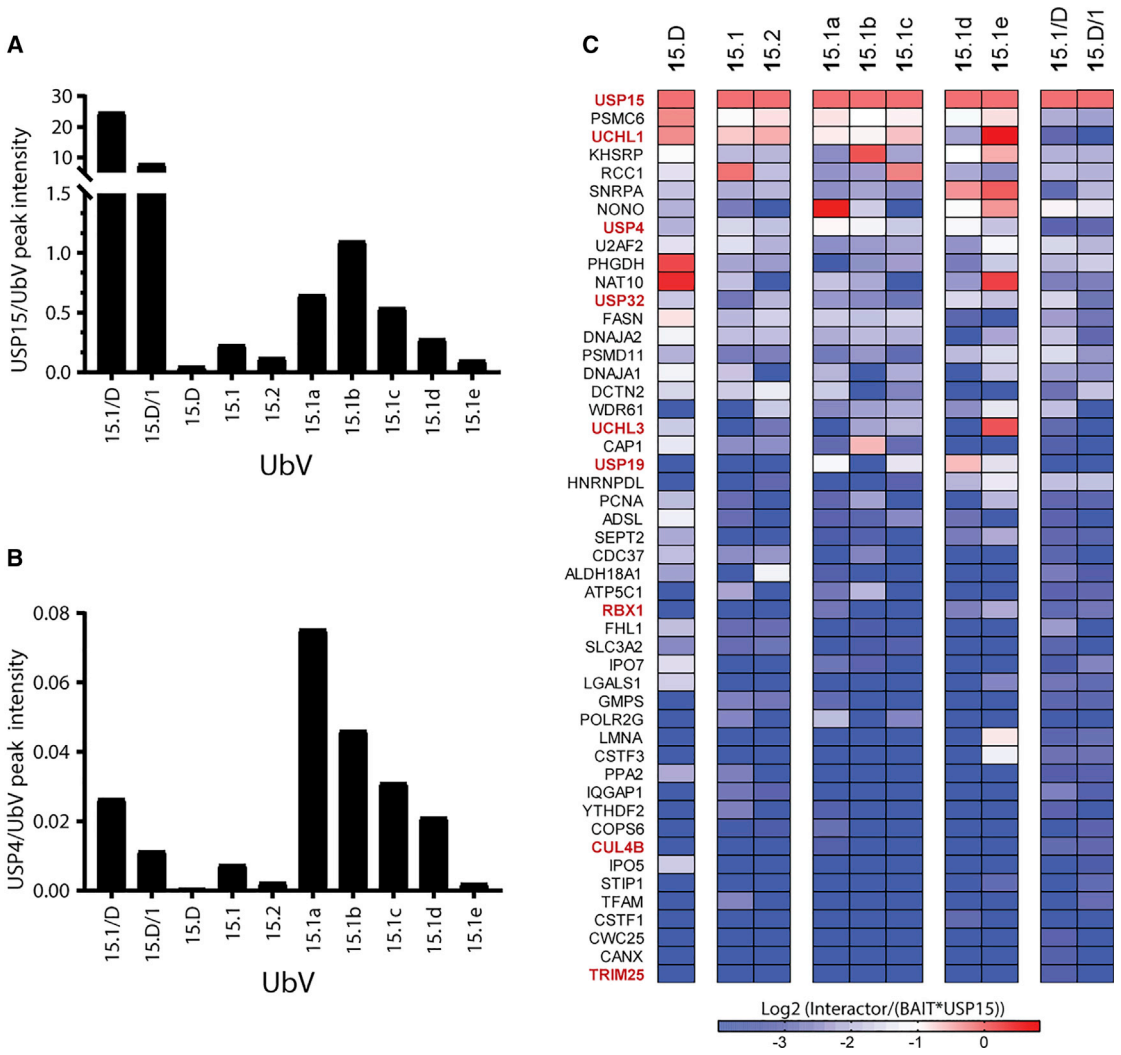

Figure 3. Mass Spectrometry of Cellular Proteins Co-precipitated with UbVs

(A and B) Mass spectrometry peak intensity ratios are shown (y axis) for immunoprecipitated UbVs (x axis) and co-immunoprecipitated USP15 (A) or USP4 (B). (C) Heatmap representation of the signal intensities for co-precipitated proteins which satisfied the criteria of exhibiting a fold change >10 compared with negative control and not being a contaminant that interacted with anti-FLAG antibody (Mellacheruvu et al., 2013). The signal is calculated as the intensity ratio between the interactor and the product of the UbV bait and USP15, and the interactors are ranked based on average intensities across experiments. Known USP15 physical interactors based on Pathway Commons (Cerami et al., 2011) are shown in black and ubiquitin-related enzymes in red, and the full list of interactors can be found in Table S2.

contained in the fusion (15.1 and 15.D), exhibiting good selectivity for USP15 over USP4, and not precipitating any other USPs (Figure 3C and Table 1). Together, the UbVs co-precipitated a total of 167 proteins that satisfied the criteria of exhibiting a fold change >10 compared with negative control and not being a contaminant that interacted with anti-FLAG antibody (Mellacheruvu et al., 2013). Forty-eight of these 167 proteins were known to interact with USP15 (Cerami et al., 2011), and 23 of these were co-precipitated with the diUbVs (Table S2). Notably, the normalized intensity signal for the diUbV interactors were generally lower than those for the UbV interactors, and the diUbVs did not show any high-signal interactors other than USP15 (>−1 score cutoff, Figure 3C), suggesting that the diUbVs are more specific than the monomeric UbVs.

In addition to USP15, five other DUBs from two structural subfamilies (USP4, USP19, USP32, UCHL1, and UCHL3) were co-precipitated with the various inhibitors, although co-precipitation of these other DUBs was much less efficient with the diUbVs compared with the UbVs. Thus, to further assess the potency and selectivity of the UbVs, we performed *in vitro* activity assays for 11 human DUBs (Table 1), including three that co-immunoprecipitated with UbVs (USP4, USP19, and UCHL1). The results further confirmed the high specificity of the diUbVs and first-generation UbVs 15.1 and 15.2, which only inhibited USP15 and USP4. In contrast, the second- and third-generation UbVs also exhibited appreciable inhibition of USP11 and USP19. The results validated the IP-MS data, as none of the UbVs inhibited five USPs that were not identified by co-precipitation

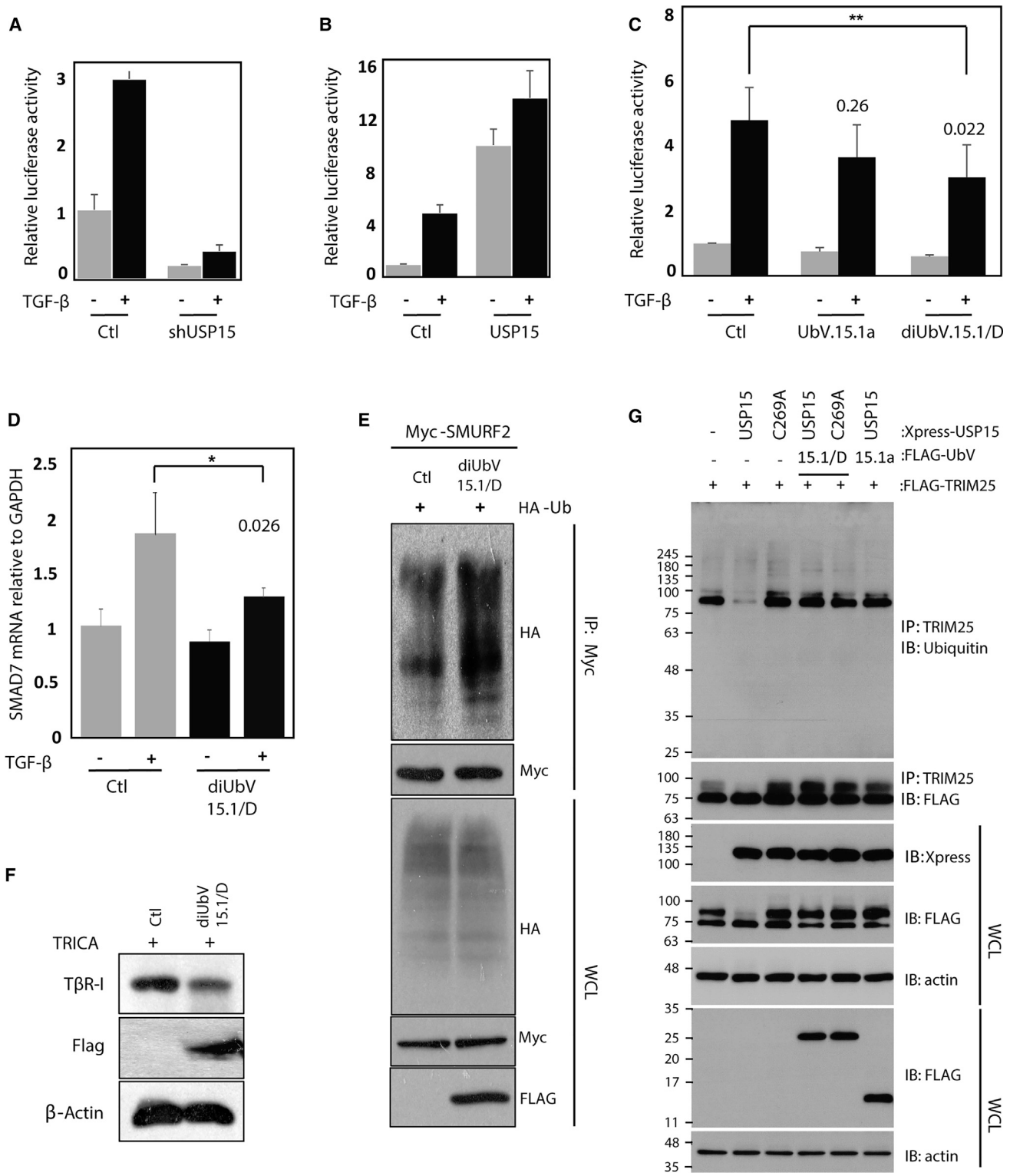

Figure 4. Biological Activity of UbVs in HEK293T Cells

(A–C) CAGA-Luc reporter assays. Cells were transfected with plasmids to express the CAGA-Luc reporter and either (A) shRNA targeting USP15 or shRNA targeting the mouse-specific B subunit PR59 (Ctl), (B) USP15 or empty vector (Ctl), and (C) UbV,15.1a, diUbV.15.1/D or empty vector (Ctl). After 48 h, cells were treated with TGF-β (2.5 ng/mL) for 16 h and the luciferase assay was performed. Data are mean ± SD (n = 3, **$p < 0.05$).

(D) Assessment of SMAD7 mRNA levels. Cells were transfected with an empty vector (Ctl) or a vector expressing diUbV.15.1/D. After 48 h, cells were treated with TGF-β (2.5 ng/mL) for 3 h. SMAD7 mRNA levels relative to GAPDH were determined by real-time qPCR. Data are mean ± SD (n = 3, *$p < 0.05$).

(legend continued on next page)

(USP2, USP7, USP8, USP9x, and USP28). Moreover, none of the UbVs inhibited UCHL1, even though this DUB was co-precipitated with some UbVs, suggesting that it may interact indirectly with UbVs or that it may bind UbVs in a manner that does not affect catalytic activity. Taken together, the IP-MS and *in vitro* enzymatic assays show that optimization of monomeric UbVs enhanced efficiency of interactions with USP15 but also exacerbated non-specific interactions, whereas coupling two specific USP15 binders in a diUbV format enhanced affinity without compromising specificity.

Effects of UbVs on USP15 Function in Cells

To assess the ability of UbVs to inhibit USP15 function in cells, we analyzed the effects of UbV expression on a known pathway involving USP15. USP15 targets several nodes in the TGF-β pathway (Eichhorn et al., 2012; Inui et al., 2011; Iyengar et al., 2015; Zhang et al., 2012), and we explored how UbVs affected TGF-β signaling and intracellular components of the pathway. As part of a negative feedback loop, SMAD7 is transcriptionally induced by TGF-β and downregulates TGF-β signaling by recruiting SMURF2 to the TGF-β receptor complex to facilitate receptor ubiquitination and complex degradation (Yan et al., 2009). USP15 forms a ternary complex with SMAD7 and SMURF2, and upon recruitment to the TGF-β receptor complex counteracts the inhibitory effects of SMURF2 by deubiquitinating SMURF2 and its substrate TβR-I, resulting in TβR-I stabilization (Iyengar et al., 2015).

Consistent with previous reports (Iyengar et al., 2015), knockdown of USP15 with short hairpin RNA (shRNA) (Figure 4A) or overexpression of USP15 (Figure 4B) markedly repressed or enhanced, respectively, the activity of a TGF-β-responsive luciferase reporter (CAGA-Luc) in HEK293T cells. Similarly, co-transfection of HEK293T cells with a plasmid expressing a UbV along with the CAGA-Luc reporter, in the presence of TGF-β, resulted in 20% or 40% inhibition of luciferase activity for UbV.15.1a or diUbV.15.1/D, respectively (Figure 4C). Also consistent with inhibition of the TGF-β pathway, expression of diUbV.15.1/D reduced levels of *SMAD7* mRNA (Figure 4D), a gene that is turned on in response to TGF-β signaling (Nakao et al., 1997). To directly assess the effects of diUbV.15.1/D on SMURF2 ubiquitination, we co-transfected HEK293T cells with expression plasmids for Myc-tagged SMURF2, hemagglutinin (HA)-tagged Ub.wt, and FLAG-tagged diUbV.15.1/D. As expected for inhibition of USP15, immunoprecipitation of SMURF2 followed by immunoblotting for Ub revealed increased ubiquitination in the presence of diUbV.15.1/D (Figure 4E). Also, consistent with USP15 inhibition and consequent increase in SMURF2 activity, levels of the SMURF2 substrate TβR-I were decreased in HEK293T cells transfected with a plasmid expressing diUbV.15.1/D (Figure 4F). We also examined the effects of UbVs on the ubiquitination of the USP15 substrate TRIM25, a potential oncogene in colorectal cancer (Sun et al., 2017) that activates the TGF-β pathway by promoting phosphorylation of SMAD2 and SMAD4. We co-transfected HEK293T cells with expression plasmids encoding FLAG-tagged TRIM25, USP15, and various FLAG-tagged UbVs, then used western blotting to assess ubiquitination of immunoprecipitated TRIM25 (Figure 4G). As expected, exogenous expression of wild-type USP15 markedly decreased the ubiquitination of TRIM25 compared with that in HEK293T cells expressing empty plasmid (pcDNA3.1/nFLAG) or a catalytically inactive USP15 mutant (C269A, Figure 4G). Confirming the potency of our USP15 inhibitors, overexpression of UbV.15.1a or diUbV.15.1/D significantly increased TRIM25 ubiquitination to levels comparable with those of the negative controls. Overall, these studies confirmed that UbVs, and diUbV.15.1/D in particular, acted as strong inhibitors of USP15 in cells as evidenced by increased ubiquitination of USP15 substrates and inhibition of signaling through the TGF-β pathway.

Crystal Structures of UbVs in Complex with USP15 Protein Fragments

To better understand the molecular basis for the binding and inhibitory effects of the UbVs, we attempted to solve the crystal structure of diUbV.1/D in complex with USP15 FLΔinsert. However, we were unsuccessful in obtaining crystals, likely due to the flexibility of the diUbV.1/D linker and some regions of the USP15 protein. Thus, we adapted an alternative strategy aimed at solving independently the structures of UbV.15.D in complex with the DUSP domain and various UbVs in complex with the D1D2 domain. We were successful in solving the UbV.15.D/DUSP structure at 3.1-Å resolution (Table 2). In the case of the D1D2 domain, we attempted to improve crystallization by truncating putative flexible regions. Eventually, we constructed a version of the D1D2 domain that lacked the C-terminal residues 934–981 (D1D2Δ1) and another version that also lacked residues 780–863 (D1D2Δ2), and although we could not solve the structure of UbV.15.1 in complex with any of the D1D2 proteins, we did solve the structure of UbV.15.2 in complex with D1D2Δ1 and the structures of UbVs 15.1a and 15.1d in complex with D1D2Δ2 at 2.5-, 1.9-, and 2.0-Å resolution, respectively (Table 2).

Molecular Interactions between the USP15 DUSP Domain and UbV.15.D

The asymmetric unit of the UbV.15.D/DUSP complex contained six DUSP molecules and six UbV molecules arranged as three tetramers. Unexpectedly, the structure revealed that two UbV.15.D monomers form a strand-swapped dimer that engages two DUSP domains simultaneously (Figure 5A), and gel-filtration

(E) Assessment of SMURF2 ubiquitination by western blotting. Cells were transfected with vectors expressing Myc-tagged SMURF2 (Myc-SMURF2), hemagglutinin (HA)-tagged Ub (HA-Ub), and diUbV.15.1/D. Whole-cell lysates (WCLs) were subjected to immunoprecipitation with an anti-Myc antibody and blots were probed with an anti-HA antibody to detect ubiquitinated SMURF2.

(F) Assessment of TβR-I levels by western blotting. Cells were transfected with a vector expressing constitutively active TβR-I (TRICA) and an empty vector (Ctl) or a vector expressing FLAG-tagged diUbV.15.1/D, and treated overnight with TGF-β (2.5 ng/mL). WCL blots were probed with the indicated antibodies.

(G) Assessment of TRIM25 ubiquitination by western blotting. Cells were transfected with vectors expressing FLAG-tagged TRIM25 (FLAG-TRIM25) and either Xpress-tagged wild-type USP15 (USP15) or a catalytically inactive USP15 mutant (C269A), with or without plasmids expressing FLAG-tagged diUbV.15.1/D or UbV.15.1a. After 24 h, WCLs were subjected to immunoprecipitation with an anti-TRIM25 antibody and probed with the indicated antibodies.

Table 2. Structure Data Collection and Refinement Statistics of Protein Complexes

	USP15-DUSP/UbV.15.D	USP15-D1D2/UbV.15.2	USP15-D1D2/UbV.15.1a	USP15-D1D2/UbV.15.1d
PDB ID	6DJ9	6CRN	6ML1	6CPM
Data Collection				
Beamline	NECAT-24-ID-E	NECAT-24-ID-C	NECAT-24-ID-E	Rigaku MicroMax007
Wavelength (Å)	0.97918	0.97920	0.97918	1.54178
Crystals	Native	Native	Native	Native
Unit cell parameters				
Space group	*P63*[a]	*P1*	*P21*	*P21*
a, *b*, *c* (Å)	152.4,152.4,125.5	41.8,98.9,122.0	42.8, 115.3, 95.3	42.6,115.1,95.7
α, β, γ (°)	90, 90,120	66.5,88.3,78.1	90, 91.9, 90	90, 92.5, 90
Resolution (Å)	90.9–2.93 (3.09–2.93)	111.7–2.11 (2.15–2.11)	95.3–1.90 (1.94–1.90)	50–2.01 (2.08–2.01)
Unique reflections	69,830 (10,150)	92,086 (3,149)	71,233 (3,864)	60,994 (6,036)
Completeness (%)	100 (100)	91.2 (63.5)	98.1 (81.6)	99.5 (99.0)
R_{merge}	0.102 (1.463)	0.080 (0.826)	0.037 (0.317)	0.067 (0.507)
Overall $I/\sigma I$	8.8 (1.2)	7.6 (0.8)	15.5 (2.9)	23.4 (3.0)
Multiplicity	5.3 (5.4)	2.1 (1.9)	3.9 (3.2)	3.7 (3.5)
Wilson *B* factor	90.34	31.00	24.86	25.67
Refinement				
Resolution (Å)	90.9–3.10	111.7–2.50	49.3–1.90	38.2–2.01
R_{work}/R_{free}	0.253/0.267	0.188/0.236	0.189/0.0220	0.167/0.212
RMSD bond length (Å)	0.003	0.008	0.007	0.007
RMSD bond angle (°)	0.65	1.25	0.82	087
No. of protein atoms	9,759	13,135	6,468	6,691
No. of water atoms	0	317	393	534
B-factor average	112.0	52.3	37.0	32.8
B-factor protein	112.0	52.5	36.6	32.3
Ramachandran statistics (MolProbity)				
Preferred (%)	86.2	97.4	98.3	98.9
Allowed (%)	13.8	2.4	1.7	1.1
Disallowed (%)	0	0.2	0	0
Clashscore	16.0	8.81	2.27	3.16

Values in parentheses represent highest-resolution shell.
[a]Data were processed as *P3*, and refined in *P63*.

chromatography suggested that the free UbV.15.D exists as a dimer in solution (Figure S5). Although the overall fold of UbV.15.D is very similar to that of Ub.wt (root-mean-square deviation [RMSD] = 0.84 Å, using 72 α atoms, Figure S6A), the β1 strand of the UbV is flipped 180° from the core of the molecule such that it interacts with a second UbV′ and its place in the UbV structure is taken by the β1′ strand. Consequently, an intermolecular, anti-parallel β sheet is formed by β1-β2 interacting with β1′-β2′, and this surface forms a groove that cradles the DUSP domains. This configuration may in part explain the high affinity of the interaction and the improved potency of the diUbV inhibitors compared with UbV.15.1, as bivalent avidity effects typically enhance apparent affinities. A similar dimeric arrangement was observed previously in the structure of a different UbV (UbV.XRD) in complex with a RING E3 ligase, and in that case dimerization of the UbV was constitutive and required for activation of the ligase (Gabrielsen et al., 2017). In contrast to the angle of 180° between the two UbVs in the UbV.XRD dimer, the monomers in the UbV.15.D dimer bend about 10° downward to engage the target (Figure S6B). UbV.15.D and UbV.XRD do not share any common substitutions relative to Ub.wt and differ in 21 positions that are mostly located in the strand-exchanged dimerization region (Figure S6C), but nonetheless both UbV dimers use similar surfaces to recognize their respective binding partners (Figure S6D).

The DUSP structure, which is composed of a three-strand anti-parallel β sheet supported by a bundle of three α helices, is nearly identical to a previous structure of the USP4 DUSP domain (RMSD = 1.24 Å, for 110 α atoms, Figure S6E) (de Jong et al., 2006). The two DUSP domains use nearly identical surfaces to interact with the UbV.15.D dimer, which are different from the surface used by the USP15 DUSP domain to bind the spliceosome recruiting factor SART3 (Figure S6F) (Zhang et al., 2016a). Here we describe the interactions between DUSP (rather than DUSP′) and the UbV.15.D dimer, which result in the burial of 821 and 1,696 Å^2 of surface area, respectively (Figure 5B). On the UbV side, roughly half of the structural epitope (799 Å^2) is contributed by residues that are substituted relative to Ub.wt

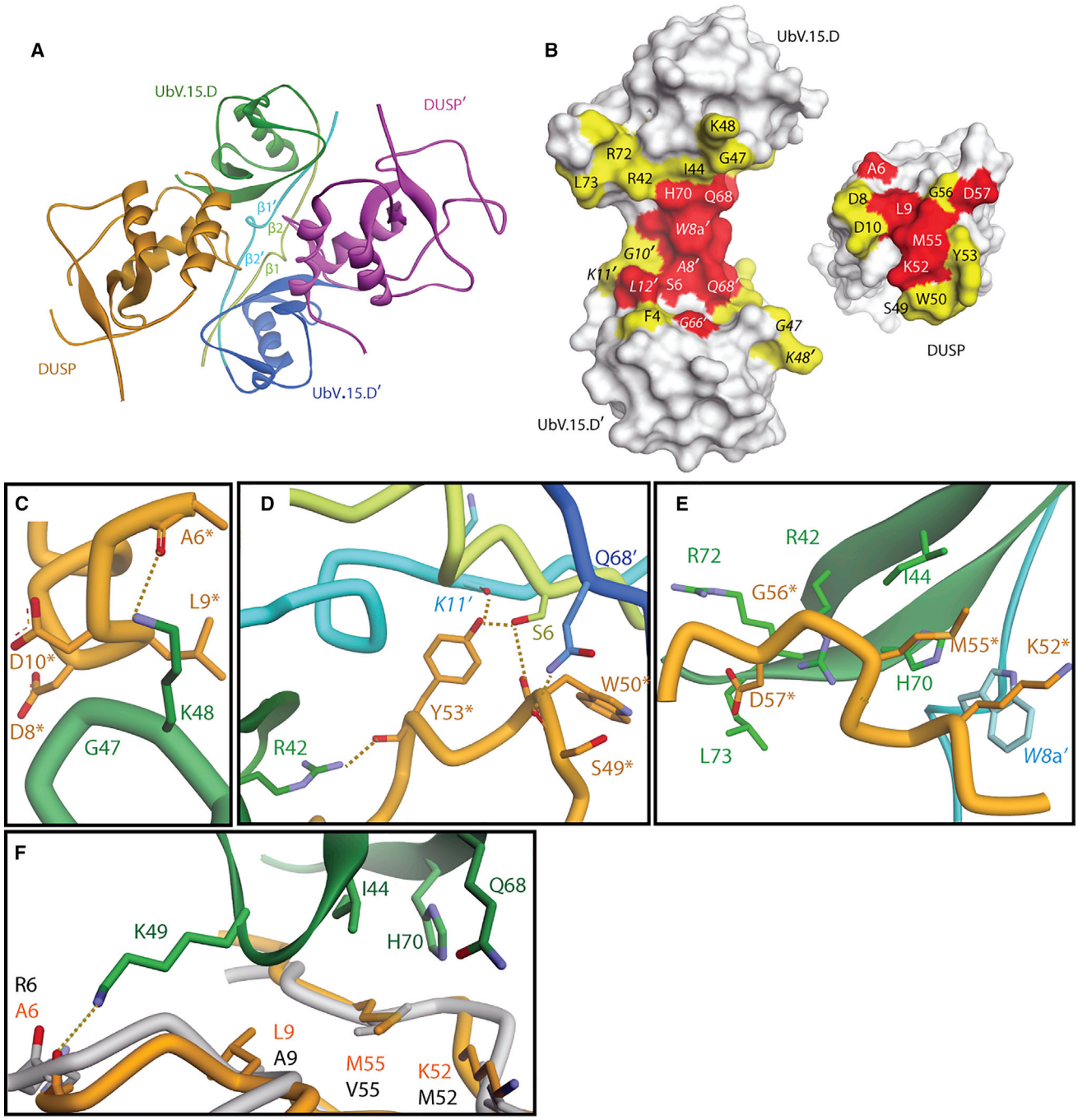

Figure 5. Structure of UbV.15.D Dimer in Complex with USP15 DUSP Domains

(A) Ribbon representation of the crystal structure of a strand-swapped UbV.15.D dimer in complex with two DUSP domains. DUSP and DUSP′ are colored orange and pink, respectively. The UbV.15.D dimer is formed by a β1-strand swap between UbV.15.D (green) and UbV.15.D′ (blue), which results in the formation of an intermolecular β sheet formed by the β1-β2 strand (light green) and the β1′-β2′ strand (light blue).

(B) Open-book view of the complex with the UbV.15.D dimer (left) and the DUSP monomer (right). The proteins are shown as molecular surfaces with non-contact residues colored gray. Residues on UbV.15.D that are substituted or conserved relative to Ub.wt, and residues on the DUSP domain that contact substituted or conserved residues on UbV.15.D, are colored red or yellow, respectively.

(C–E) Close-up views of the molecular interactions between the UbV.15.D dimer and the DUSP domain N-terminal region (C) and α2-β2 loop region (D and E).

(F) Superposition of DUSP structures of USP4 (gray; PDB: 5CRT) and USP15 bound to UbV.15.D. In (C) to (F) the main chains are shown as ribbons and side chains are shown as sticks colored as in (A). DUSP residues are numbered according to the USP15 PDB numbering, whereas UbV residues are numbered according to alignment with the sequence of Ub.wt.

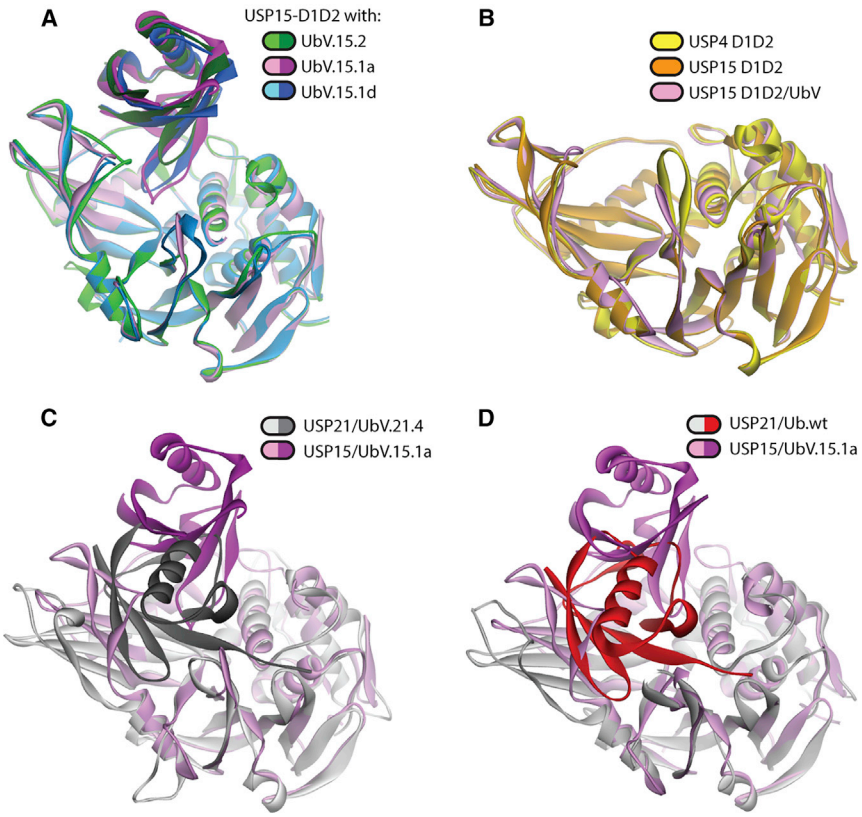

Figure 6. Comparison of Structures of USP15 D1D2 in Complex with UbVs and Other USPs

(A–D) Superposition of structures of: (A) USP15 D1D2 in complex with UbV.15.2 (green), UbV.15.1a (pink), or UbV.15.1d (blue); (B) USP15 D1D2 from the complex with UbV.15.1a (pink), apo USP4 D1D2 (yellow, PDB: 2Y6E), and apo USP15 D1D2 (orange, PDB: 6GHA); (C) USP15 D1D2 in complex with UbV.15.1a (pink) and USP21 in complex with UbV.21.4 (gray, PDB: 3MTN); (D) USP15 D1D2 in complex with UbV.15.1a (pink) and USP21 in complex with Ub.wt (red, PDB: 2Y5B).

and form a contiguous patch in the center of the epitope. The DUSP epitope can be divided into two regions. The first region consists of four residues in the N-terminal region (Ala^{6*}, Asp^{8*}, Leu^{9*}, Asp^{10*}; DUSP residues are denoted by asterisks) that pack against Gly^{47} and Lys^{48} on the first UbV.15.D monomer, facilitating a hydrogen bond between the side chain of Lys^{48} and the main chain of Ala^{6*} and long-range electrostatic interactions with the side chains of Asp^{8*}and Asp^{10*} (Figure 5C). The second region, contained within the DUSP β1-β2 loop (residues 49*–57*), makes hydrophobic and polar contacts with the UbV dimer. The main chain of Ser^{49*}, Trp^{50*}, and Tyr^{53*} and the side chain of Tyr^{53*} form a hydrogen-bond network with the side chains of Ser^{6} and Arg^{42} in UbV.15.D and the main chain of Lys$^{11'}$ and the side chain of Gln$^{68'}$ on UbV.15.D′ (Figure 5D), and Lys^{52*}, Met^{55*}, Gly^{56*}, and Asp^{57*} pack against Arg^{42}, Ile^{44}, His^{70}, Arg^{72}, Leu^{73}, and Trp$^{8a'}$ (Figure 5E).

The structure also explains the specificity of UbV.15.D (Figure 2B), as the DUSP domains of USP15 and USP4 differ at four positions (6*, 9*, 52*, and 55*), and these differences are likely to compromise complementarity at the interface in the case of USP4 compared with USP15 (Figure 5F). Superposition of the structure of the DUSP domain of USP4 with that of USP15 in complex with UbV.15.D shows differences in the N-terminal regions of the DUSP domains that could affect the hydrogen-bond interaction between the Lys^{49} side chain of the UbV and the carboxyl group of residue 6*, which is Ala or Arg in USP15 or USP4, respectively. In addition, residues 9* and 55*, which are Leu or Ala, and Met or Val in USP15 or USP4, respectively, form a smaller hydrophobic patch in USP4 compared with USP15, which would likely reduce favorable packing with Ile^{44} and His^{70} of UbV.15.D. Finally, residue 52* is Lys or Met in USP15 or USP4, respectively, and this may compromise the ability of USP4 to form hydrogen-bond interactions with the Gln^{68} side chain of UbV.15.D.

Molecular Interactions between USP15 D1D2 and UbVs 15.2, 15.1a, and 15.1d

The structures of UbVs 15.2, 15.1a, and 15.1d in complex with USP15 D1D2 all showed similar binding modes and conformations (pairwise RMSD = 0.70–0.90 Å, for 378–389 α atoms), with the UbVs binding to the occluded ''closed-hand'' conformation of USP15 D1D2 (Figure 6A). Superposition of a representative USP15 D1D2 structure (from the complex with UbV.15.1a) with the structure of free USP15 D1D2 (Ward et al., 2018) or USP4 D1D2 (Clerici et al., 2014) showed high similarity (RMSD = 0.82 or 0.61 Å, respectively, for 308 α atoms, Figure 6B). Superposition of the structure of UbV.15.1a in complex with USP15 D1D2 with that of UbV.21.4 in complex with USP21 (Ernst et al., 2013), an example of a UbV inhibitor bound to a USP in an active conformation, revealed very significant differences in the positions of the UbVs (Figure 6C). In particular, whereas UbV.21.4 is nested deep within the Ub-binding site of USP21 in a manner nearly identical to that of substrate Ub.wt (Figure 6D) (Ernst et al., 2013), UbV.15.1a sits on top of the closed Ub-binding site of USP15 D1D2. Taken together, these results show that UbVs 15.2, 15.1a, and 15.1d bind to the closed form of USP15 D1D2 and likely act as inhibitors by stabilizing this inactive conformation and blocking access of substrate Ub to the active site.

The interface between UbV.15.2 and USP15 D1D2 is of moderate size, with 703 and 751 Å^2 buried on UbV.15.2 and USP15, respectively, and each epitope is composed of two non-contiguous patches (Figure 7A). UbVs 15.1a and 15.1d make contacts similar to those made by UbV.15.2, but their extended β3-β4 loops form additional contacts and form larger and more contiguous interfaces with burial of significantly more surface area: 1,184 and 1,070 Å^2 for UbV.15.1a and D1D2, respectively (Figure 7B), and 916 and 879 Å^2 for UbV.15.1d and D1D2, respectively (Figure 7C). Although UbV.15.2 contains six substitutions relative to Ub.wt, only two of these (Phe^{12} and Tyr^{64}) interact

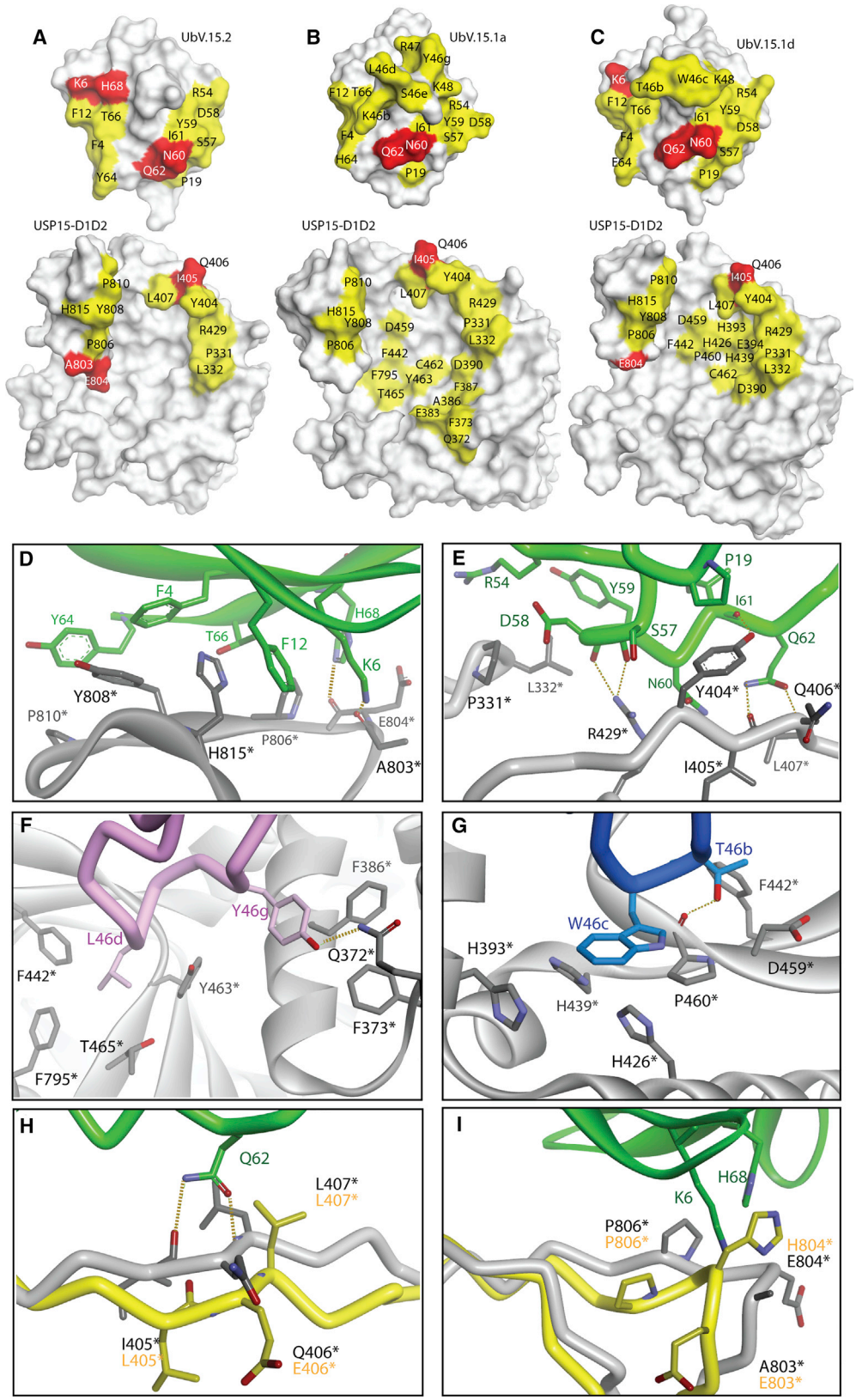

(legend on next page)

with D1D2, and together with four conserved residues (Phe^{4}, Lys^{6}, Thr^{66}, and His^{68}), form a patch (patch 1) that packs against the zinc-finger region of USP15 (Figure 7D). Notably, Phe^{12} and Tyr^{64} form favorable interactions with Pro^{806*}and His^{815*}, or with Tyr^{808*} and Pro^{810*}, respectively, which would not be achieved by the smaller and more hydrophilic Thr^{12} and Glu^{64} residues of Ub.wt. A second interaction patch (patch 2) is formed by eight UbV.15.2 residues, which are conserved with Ub.wt and interact with seven residues of D1D2 (Figure 7E).

UbV.15.1a makes contacts with D1D2 regions similar to those engaged by UbV.15.2, but these are augmented by additional contacts made by the extended β3-β4 loop (Figure 7B). The Leu^{46d} side chain at the tip of the β3-β4 loop packs against a hydrophobic cluster consisting of Phe^{442*}, Tyr^{463*}, Thr^{465*}, and Phe^{795*}, and the Tyr^{46g} side chain packs against the aromatic side chains of Phe^{373*} and Phe^{387*} and forms a hydrogen bond with the side chain of Gln^{372*} (Figure 7F). UbV.15.1d also augments interactions that resemble those of UbV.15.2 with interactions mediated by its extended β3-β4 loop, but these differ significantly from those of UbV.15.1a. At the tip of the β3-β4 loop, Trp^{46c} packs against Pro^{460*} and a cluster of three His side chains (His^{393*}, His^{426*}, and His^{460*}), and Thr^{46b} packs against Phe^{442*} and Asp^{459*} and forms a hydrogen bond with the Pro^{460*} main chain (Figure 7G).

USP15 D1D2 differs from USP4 at four positions that interact with UbV.15.2 (405*, 406*, 803*, and 804*), and thus interactions involving some of these positions likely explain the specificity of UbV.15.2 for USP15 over USP4 (Figure 7A). Superposition of the structure of USP4 D1D2 with that of USP15 D1D2 in complex with UbV.15.2 shows conformational differences in the region containing residues 405* and 406* that could affect hydrogen-bond interactions with Gln^{62} of UbV.15.2 (Figure 7H). Similarly, significant conformational differences in the zinc-finger region affect residues 803* and 804*, which are Ala or Glu, and Glu or His in USP15 or USP4, respectively (Figure 7I). Specifically, differences in the main-chain conformation place Glu^{804*} of USP15 away from the interface with UbV.15.2, whereas docking of the superposed USP4 structure suggests that His^{804*} of USP4 would clash sterically with Lys^{6} and His^{68} of UbV.15.2, and Pro^{806*} of USP4 would not be able to pack against Lys^{6} of UbV.15.2. However, since our structure of USP15 D1D2 is in complex with UbV.15.2, whereas the reported structure of USP4 D1D2 is unbound, it is not clear whether these conformational differences are intrinsic or caused by UbV.15.2 binding. Regardless, despite having larger interfaces, UbVs 15.1a and 15.1d do not interact as significantly with Glu^{804*} and the surrounding region of USP15, but instead make more extensive contacts with regions of USP15 that are conserved with USP4 (Figures 7B and 7C). Taken together, these structural comparisons suggest that the selectivity of UbV.15.2 for USP15 over USP4 may be due to interactions with the divergent USP position 804*. In contrast, UbVs 15.1a and 15.1d interact extensively with regions of USP15 that are conserved with USP4 but not with position 804*, and thus inhibit both USP15 and USP4 with high potency (Table 1).

DISCUSSION

USP15 is a widely expressed DUB that regulates diverse cellular processes and has been associated with cancer and other diseases (Fielding et al., 2018). Understanding of USP15 biology has been limited by insufficient knowledge of the molecular mechanisms of its activity and regulation, and thus specific inhibitors of enzyme activity are needed to probe the consequences of USP15 inhibition. However, designing small-molecule inhibitors for USP15 and many other DUBs remains extremely challenging because of their multi-domain nature and complex regulatory mechanisms that affect catalytic activity (Harrigan et al., 2018). We used a recently established phage display strategy (Ernst et al., 2013) to engineer high-affinity UbVs that selectively bound distinct regions of USP15, including the DUSP domain, the two Ubl domains, and the catalytic domain. To improve potency of inhibition, we diversified and extended the UbV β3-β4 loop to increase interactions with the USP15 catalytic site. In addition, we exploited the modularity of UbVs to develop dimeric diUbVs to target the catalytic and DUSP domains simultaneously. The diUbVs proved to be potent and specific inhibitors of USP15 in cells, where they affected the activity of USP15 substrates and modulated the TGF-β pathway. Due to structural similarity and functional overlap between USP15 and USP4 (Vlasschaert et al., 2015), we cannot completely rule out inhibition of USP4 by the UbVs. However, UbVs that target both enzymes may also prove useful to explore consequences of inhibiting both enzymes simultaneously.

Structural and biochemical studies of USP15/UbV complexes provided several important insights into the functions of USP15 and UbV inhibitors. First, we observed that UbVs bound on top of the occluded Ub-binding site of the USP15 catalytic domain, and thus inhibited the enzyme by reinforcing the closed, inactive conformation observed in the apo structures of the catalytic domains of USP15 (Ward et al., 2018) and USP4 (Clerici et al., 2014). Second, the extended β3-β4 loops of UbVs made additional contacts with the USP15 catalytic domain, which enhanced affinity but compromised specificity relative to USP4. Third, an unexpected β1-strand swap caused UbV.15.D to form an unusual dimer that provided a new binding surface that could

Figure 7. Molecular Interactions between USP15 D1D2 and UbVs

(A–C) Open-book views of the USP15 D1D2 domain (bottom) in complex with (A) UbV.15.2, (B) UbV.15.1a, or (C) UbV.15.1d (top). The proteins are shown as molecular surfaces with non-contact residues colored gray. Residues on USP15 that are conserved or different compared with USP4, and residues on UbVs that contact conserved or different residues on USP15, are colored yellow or red, respectively.

(D–G) Close-up views of the molecular interactions of USP15 with (D) patch 1 of UbV.15.2, (E) patch 2 of UbV.15.2, (F) the β3-β4 loop of UbV.15.1a, and (G) the β3-β4 loop of UbV.15.1d.

(H and I) Close-up views of the superposition of D1D2 structures of USP4 and USP15 bound to UbV.15.2 on patch 2 (H) and patch 1 (I). Main chains are shown as ribbons and side chains are shown as sticks. USP15 is colored gray, USP4 is colored yellow, and UbVs 15.2, 15.1a, and 15.1d are colored green, pink, and blue, respectively. USP15 and USP4 residues are numbered according to the USP15 PDB numbering, whereas UbV residues are numbered according to alignment with the sequence of Ub.wt (see Figure 2).

interact tightly and specifically with the USP15 DUSP domain. Our results suggest that diUbVs likely interact simultaneously with DUSP and catalytic domains, and the domain-swapped dimer may facilitate simultaneous binding to two USP15 molecules, thus generating avidity effects that could enhance affinity.

A powerful aspect of phage display technology is that libraries can be improved in response to insights gained from the results of selection experiments, functional analyses, and structural information. Structures of the UbVs studied here will inform designs for new libraries utilizing the β1-strand swap and extensions in the β1-β2 and β3-β4 loops to develop more potent, specific, and functionally diverse UbVs for targeting the myriad components of the UPS. Moreover, the human proteome contains numerous Ubl domains with a wide range of sequence and length diversity in the β1-β2 and β3-β4 loop regions (van der Veen and Ploegh, 2012), and it is intriguing to speculate that some Ubl domains may be naturally predisposed to form dimers through a β1-strand swap or may utilize divergent loops to interact with and regulate DUBs and other UPS enzymes.

In summary, by applying a pipeline encompassing phage display, enzymology, structural analysis, and cell-based assays, we developed potent and specific UbV inhibitors for the complex DUB USP15. Our work yielded the most potent and selective intracellular inhibitors of USP15 reported thus far, and the results demonstrated the power and versatility of the UbV engineering platform. We anticipate that these UbVs will be useful tools for studying the many signaling pathways associated with USP15 and for facilitating the development of therapeutic drugs.

STAR★METHODS

Detailed methods are provided in the online version of this paper and include the following:

- KEY RESOURCES TABLE
- CONTACT FOR REAGENT AND RESOURCE SHARING
- EXPERIMENTAL MODEL AND SUBJECT DETAILS
  - Recombinant Proteins
  - Cell Culture
- METHOD DETAILS
  - Library Construction
  - Protein Expression and Purification
  - Phage-Displayed UbV Selections
  - ELISAs to Evaluate Binding and Specificity
  - Enzyme Activity and Inhibition Assays
  - Protein Purification for Crystallization and Structure Determination
  - Plasmids for Mammalian Cell Experiments
  - Immunoprecipitation and Mass Spectrometry
  - Luciferase-Based TGF-β Reporter Assay
  - Quantitative Real-Time PCR (qRT-PCR)
  - Immunoprecipitation and In Vivo Deubiquitination Assays
- DATA AND SOFTWARE AVAILABILITY

SUPPLEMENTAL INFORMATION

Supplemental Information includes six figures and two tables and can be found with this article online at https://doi.org/10.1016/j.str.2019.01.002.

ACKNOWLEDGMENTS

We are grateful to D. Wyatt and M. Sartori for insightful discussions. We also thank L. Beatty, J. Gu, M. Sartori, D. Haddad, I. Leung, I. Kourniov, E. Marcon, and H. Guo for technical assistance. Diffraction experiments were performed at the Advanced Photon Source on the Northeastern Collaborative Access Team beamlines. This work was financially supported by the Boehringer Ingelheim, and in part by the National Research Foundation Singapore and the Singapore Ministry of Education under its Research Centers of Excellence initiative.

AUTHOR CONTRIBUTIONS

Conceptualization, M.L., G.B., and S.S.S.; Methodology, J.Teyra, A.U.S., F.W.S., P.G., P.J.A.E., M.L., G.B., and S.S.S.; Investigation, J.Teyra, J.Tong, A.U.S., F.W.S., P.J., S.K.L.L., M.J.P., N.F., C.S., B.B.B., D.F.J.C., and J.R.K.; Writing – Original Draft, A.U.S., J.Teyra, P.G., P.J.A.E., and S.S.S.; Writing – Editing and Reviewing, J.Teyra and S.S.S.; Supervision, F.S., J.M., M.F.M., P.G., P.J.A.E., M.L., G.B., and S.S.S.; Funding Acquisition, S.S.S., M.L., and G.B.

DECLARATION OF INTERESTS

This study was funded by a sponsored research agreement with Boehringer Ingelheim. The authors declare no competing interests.

Received: July 16, 2018
Revised: October 23, 2018
Accepted: December 31, 2018
Published: January 31, 2019

REFERENCES

Battye, T.G.G., Kontogiannis, L., Johnson, O., Powell, H.R., and Leslie, A.G.W. (2011). iMOSFLM: a new graphical interface for diffraction-image processing with MOSFLM. Acta Crystallogr. D Biol. Crystallogr. *67*, 271–281.

Biasini, M., Bienert, S., Waterhouse, A., Arnold, K., Studer, G., Schmidt, T., Kiefer, F., Gallo Cassarino, T., Bertoni, M., Bordoli, L., et al. (2014). SWISS-MODEL: modelling protein tertiary and quaternary structure using evolutionary information. Nucleic Acids Res. *42*, W252–W258.

Burroughs, A.M., Balaji, S., Iyer, L.M., and Aravind, L. (2007). Small but versatile: the extraordinary functional and structural diversity of the beta-grasp fold. Biol. Direct *2*, 18.

Cerami, E.G., Gross, B.E., Demir, E., Rodchenkov, I., Babur, O., Anwar, N., Schultz, N., Bader, G.D., and Sander, C. (2011). Pathway Commons, a web resource for biological pathway data. Nucleic Acids Res. *39*, D685–D690.

Chen, V.B., Arendall, W.B., 3rd, Headd, J.J., Keedy, D.A., Immormino, R.M., Kapral, G.J., Murray, L.W., Richardson, J.S., and Richardson, D.C. (2010). MolProbity: all-atom structure validation for macromolecular crystallography. Acta Crystallogr. D Biol. Crystallogr. *66*, 12–21.

Chou, C.-K., Chang, Y.-T., Korinek, M., Chen, Y.-T., Yang, Y.-T., Leu, S., Lin, I.-L., Tang, C.-J., and Chiu, C.-C. (2017). The regulations of deubiquitinase USP15 and its pathophysiological mechanisms in diseases. Int. J. Mol. Sci. *18*, https://doi.org/10.3390/ijms18030483.

Clague, M.J., Coulson, J.M., and Urbé, S. (2012). Cellular functions of the DUBs. J. Cell Sci. *125*, 277–286.

Clague, M.J., Barsukov, I., Coulson, J.M., Liu, H., Rigden, D.J., and Urbé, S. (2013). Deubiquitylases from genes to organism. Physiol. Rev. *93*, 1289–1315.

Clerici, M., Luna-Vargas, M.P.A., Faesen, A.C., and Sixma, T.K. (2014). The DUSP-Ubl domain of USP4 enhances its catalytic efficiency by promoting ubiquitin exchange. Nat. Commun. *5*, 5399.

Cornelissen, T., Haddad, D., Wauters, F., Van Humbeeck, C., Mandemakers, W., Koentjoro, B., Sue, C., Gevaert, K., De Strooper, B., Verstreken, P., et al. (2014). The deubiquitinase USP15 antagonizes Parkin-mediated mitochondrial ubiquitination and mitophagy. Hum. Mol. Genet. *23*, 5227–5242.

Dang, L.C., Melandri, F.D., and Stein, R.L. (1998). Kinetic and mechanistic studies on the hydrolysis of ubiquitin C-terminal 7-amido-4-methylcoumarin by deubiquitinating enzymes. Biochemistry *37*, 1868–1879.

Darling, S., Fielding, A.B., Sabat-Pośpiech, D., Prior, I.A., and Coulson, J.M. (2017). Regulation of the cell cycle and centrosome biology by deubiquitylases. Biochem. Soc. Trans. *45*, 1125–1136.

Eichhorn, P.J.A., Rodón, L., Gonzàlez-Juncà, A., Dirac, A., Gili, M., Martínez-Sáez, E., Aura, C., Barba, I., Peg, V., Prat, A., et al. (2012). USP15 stabilizes TGF-β receptor I and promotes oncogenesis through the activation of TGF-β signaling in glioblastoma. Nat. Med. *18*, 429–435.

Emsley, P., and Cowtan, K. (2004). Coot: model-building tools for molecular graphics. Acta Crystallogr. D Biol. Crystallogr. *60*, 2126–2132.

Ernst, A., Avvakumov, G., Tong, J., Fan, Y., Zhao, Y., Alberts, P., Persaud, A., Walker, J.R., Neculai, A.-M., Neculai, D., et al. (2013). A strategy for modulation of enzymes in the ubiquitin system. Science *339*, 590–595.

Fielding, A.B., Concannon, M., Darling, S., Rusilowicz-Jones, E.V., Sacco, J.J., Prior, I.A., Clague, M.J., Urbé, S., and Coulson, J.M. (2018). The deubiquitylase USP15 regulates topoisomerase II alpha to maintain genome integrity. Oncogene *37*, 2326–2342.

Gabrielsen, M., Buetow, L., Nakasone, M.A., Ahmed, S.F., Sibbet, G.J., Smith, B.O., Zhang, W., Sidhu, S.S., and Huang, D.T. (2017). A general strategy for discovery of inhibitors and activators of RING and U-box E3 ligases with ubiquitin variants. Mol. Cell *68*, 456–470.e10.

Gorelik, M., Orlicky, S., Sartori, M.A., Tang, X., Marcon, E., Kurinov, I., Greenblatt, J.F., Tyers, M., Moffat, J., Sicheri, F., et al. (2016). Inhibition of SCF ubiquitin ligases by engineered ubiquitin variants that target the Cul1 binding site on the Skp1-F-box interface. Proc. Natl. Acad. Sci. U S A *113*, 3527–3532.

Grabbe, C., Husnjak, K., and Dikic, I. (2011). The spatial and temporal organization of ubiquitin networks. Nat. Rev. Mol. Cell Biol. *12*, 295–307.

Harrigan, J.A., Jacq, X., Martin, N.M., and Jackson, S.P. (2018). Deubiquitylating enzymes and drug discovery: emerging opportunities. Nat. Rev. Drug Discov. *17*, 57–78.

Hayes, S.D., Liu, H., MacDonald, E., Sanderson, C.M., Coulson, J.M., Clague, M.J., and Urbé, S. (2012). Direct and indirect control of mitogen-activated protein kinase pathway-associated components, BRAP/IMP E3 ubiquitin ligase and CRAF/RAF1 kinase, by the deubiquitylating enzyme USP15. J. Biol. Chem. *287*, 43007–43018.

Heideker, J., and Wertz, I.E. (2015). DUBs, the regulation of cell identity and disease. Biochem. J. *467*, 191.

Huang, X., Langelotz, C., Hetfeld-Pechoc, B.K.J., Schwenk, W., and Dubiel, W. (2009). The COP9 signalosome mediates beta-catenin degradation by deneddylation and blocks adenomatous polyposis coli destruction via USP15. J. Mol. Biol. *391*, 691–702.

Inui, M., Manfrin, A., Mamidi, A., Martello, G., Morsut, L., Soligo, S., Enzo, E., Moro, S., Polo, S., Dupont, S., et al. (2011). USP15 is a deubiquitylating enzyme for receptor-activated SMADs. Nat. Cell Biol. *13*, 1368–1375.

Iyengar, P.V., Jaynes, P., Rodon, L., Lama, D., Law, K.P., Lim, Y.P., Verma, C., Seoane, J., and Eichhorn, P.J.A. (2015). USP15 regulates SMURF2 kinetics through C-lobe mediated deubiquitination. Sci. Rep. *5*, 14733.

Jarvis, D.L. (2009). Baculovirus-insect cell expression systems. Methods Enzymol. *463*, 191–222.

de Jong, R.N., Ab, E., Diercks, T., Truffault, V., Daniëls, M., Kaptein, R., and Folkers, G.E. (2006). Solution structure of the human ubiquitin-specific protease 15 DUSP domain. J. Biol. Chem. *281*, 5026–5031.

Kit Leng Lui, S., Iyengar, P.V., Jaynes, P., Isa, Z.F.B.A., Pang, B., Tan, T.Z., and Eichhorn, P.J.A. (2017). USP26 regulates TGF-β signaling by deubiquitinating and stabilizing SMAD7. EMBO Rep. *18*, 797–808.

Komander, D., Clague, M.J., and Urbé, S. (2009). Breaking the chains: structure and function of the deubiquitinases. Nat. Rev. Mol. Cell Biol. *10*, 550–563.

Kotani, Y., Morito, D., Sakata, K., Ainuki, S., Sugihara, M., Hatta, T., Iemura, S.-I., Takashima, S., Natsume, T., and Nagata, K. (2017). Alternative exon skipping biases substrate preference of the deubiquitylase USP15 for mysterin/RNF213, the moyamoya disease susceptibility factor. Sci. Rep. *7*, 44293.

Kumari, N., Jaynes, P.W., Saei, A., Iyengar, P.V., Richard, J.L.C., and Eichhorn, P.J.A. (2017). The roles of ubiquitin modifying enzymes in neoplastic disease. Biochim. Biophys. Acta *1868*, 456–483.

Lim, K.-H., Song, M.-H., and Baek, K.-H. (2016). Decision for cell fate: deubiquitinating enzymes in cell cycle checkpoint. Cell. Mol. Life Sci. *73*, 1439–1455.

Liu, W.-T., Huang, K.-Y., Lu, M.-C., Huang, H.-L., Chen, C.-Y., Cheng, Y.-L., Yu, H.-C., Liu, S.-Q., Lai, N.-S., and Huang, H.-B. (2017). TGF-β upregulates the translation of USP15 via the PI3K/AKT pathway to promote p53 stability. Oncogene *36*, 2715–2723.

Livak, K.J., and Schmittgen, T.D. (2001). Analysis of relative gene expression data using real-time quantitative PCR and the 2(-Delta Delta C(T)) method. Methods *25*, 402–408.

Long, L., Thelen, J.P., Furgason, M., Haj-Yahya, M., Brik, A., Cheng, D., Peng, J., and Yao, T. (2014). The U4/U6 recycling factor SART3 has histone chaperone activity and associates with USP15 to regulate H2B deubiquitination. J. Biol. Chem. *289*, 8916–8930.

Marcon, E., Jain, H., Bhattacharya, A., Guo, H., Phanse, S., Pu, S., Byram, G., Collins, B.C., Dowdell, E., Fenner, M., et al. (2015). Assessment of a method to characterize antibody selectivity and specificity for use in immunoprecipitation. Nat. Methods *12*, 725–731.

McCoy, A.J., Grosse-Kunstleve, R.W., Adams, P.D., Winn, M.D., Storoni, L.C., and Read, R.J. (2007). Phaser crystallographic software. J. Appl. Crystallogr. *40*, 658–674.

Mellacheruvu, D., Wright, Z., Couzens, A.L., Lambert, J.-P., St-Denis, N., Li, T., Miteva, Y.V., Hauri, S., Sardiu, M.E., Low, T.Y., et al. (2013). The CRAPome: a contaminant repository for affinity purification mass spectrometry data. Nat. Methods *10*, 730–736.

Nakao, A., Afrakhte, M., Morén, A., Nakayama, T., Christian, J.L., Heuchel, R., Itoh, S., Kawabata, M., Heldin, N.E., Heldin, C.H., et al. (1997). Identification of Smad7, a TGFbeta-inducible antagonist of TGF-beta signalling. Nature *389*, 631–635.

Olsen, J.V., Vermeulen, M., Santamaria, A., Kumar, C., Miller, M.L., Jensen, L.J., Gnad, F., Cox, J., Jensen, T.S., Nigg, E.A., et al. (2010). Quantitative phosphoproteomics reveals widespread full phosphorylation site occupancy during mitosis. Sci. Signal. *3*, ra3.

Otwinowski, Z., and Minor, W. (1997). [20] Processing of X-ray diffraction data collected in oscillation mode. Methods Enzymol. *276*, 307–326.

Persson, H., Ye, W., Wernimont, A., Adams, J.J., Koide, A., Koide, S., Lam, R., and Sidhu, S.S. (2013). CDR-H3 diversity is not required for antigen recognition by synthetic antibodies. J. Mol. Biol. *425*, 803–811.

Pinto-Fernandez, A., and Kessler, B.M. (2016). DUBbing cancer: deubiquitylating enzymes involved in epigenetics, DNA damage and the cell cycle as therapeutic targets. Front. Genet. *7*, 133.

Schweitzer, K., Bozko, P.M., Dubiel, W., and Naumann, M. (2007). CSN controls NF-kappaB by deubiquitinylation of IkappaBalpha. EMBO J. *26*, 1532–1541.

Srihari, S., and Ragan, M.A. (2013). Systematic tracking of dysregulated modules identifies novel genes in cancer. Bioinformatics *29*, 1553–1561.

Sun, N., Xue, Y., Dai, T., Li, X., and Zheng, N. (2017). Tripartite motif containing 25 promotes proliferation and invasion of colorectal cancer cells through TGF-β signaling. Biosci. Rep. *37*, https://doi.org/10.1042/BSR20170805.

Tencer, A.H., Liang, Q., and Zhuang, Z. (2016). Divergence in ubiquitin interaction and catalysis among the ubiquitin-specific protease family deubiquitinating enzymes. Biochemistry *55*, 4708–4719.

Teyra, J., Huang, H., Jain, S., Guan, X., Dong, A., Liu, Y., Tempel, W., Min, J., Tong, Y., Kim, P.M., et al. (2017). Comprehensive analysis of the human SH3 domain family reveals a wide variety of non-canonical specificities. Structure *25*, 1598–1610.e3.

Tong, J., Helmy, M., Cavalli, F.M.G., Jin, L., St-Germain, J., Karisch, R., Taylor, P., Minden, M.D., Taylor, M.D., Neel, B.G., et al. (2017). Integrated analysis of proteome, phosphotyrosine-proteome, tyrosine-kinome, and tyrosine-phosphatome in acute myeloid leukemia. Proteomics *17*, https://doi.org/10.1002/pmic.201600361.

Tonikian, R., Zhang, Y., Boone, C., and Sidhu, S.S. (2007). Identifying specificity profiles for peptide recognition modules from phage-displayed peptide libraries. Nat. Protoc. *2*, 1368–1386.

Torre, S., Polyak, M.J., Langlais, D., Fodil, N., Kennedy, J.M., Radovanovic, I., Berghout, J., Leiva-Torres, G.A., Krawczyk, C.M., Ilangumaran, S., et al. (2017). USP15 regulates type I interferon response and is required for pathogenesis of neuroinflammation. Nat. Immunol. *18*, 54–63.

Urbé, S., Liu, H., Hayes, S.D., Heride, C., Rigden, D.J., and Clague, M.J. (2012). Systematic survey of deubiquitinase localization identifies USP21 as a regulator of centrosome- and microtubule-associated functions. Mol. Biol. Cell *23*, 1095–1103.

Urzhumtsev, A., Afonine, P.V., and Adams, P.D. (2013). TLS from fundamentals to practice. Crystallogr. Rev. *19*, 230–270.

van der Veen, A.G., and Ploegh, H.L. (2012). Ubiquitin-like proteins. Annu. Rev. Biochem. *81*, 323–357.

Vizcaíno, J.A., Deutsch, E.W., Wang, R., Csordas, A., Reisinger, F., Ríos, D., Dianes, J.A., Sun, Z., Farrah, T., Bandeira, N., et al. (2014). ProteomeXchange provides globally coordinated proteomics data submission and dissemination. Nat. Biotechnol. *32*, 223–226.

Vlasschaert, C., Xia, X., Coulombe, J., and Gray, D.A. (2015). Evolution of the highly networked deubiquitinating enzymes USP4, USP15, and USP11. BMC Evol. Biol. *15*, 230.

Vos, R.M., Altreuter, J., White, E.A., and Howley, P.M. (2009). The ubiquitin-specific peptidase USP15 regulates human papillomavirus type 16 E6 protein stability. J. Virol. *83*, 8885–8892.

Wagner, S.A., Beli, P., Weinert, B.T., Nielsen, M.L., Cox, J., Mann, M., and Choudhary, C. (2011). A proteome-wide, quantitative survey of in vivo ubiquitylation sites reveals widespread regulatory roles. Mol. Cell. Proteomics *10*, M111.013284.

Ward, S.J., Gratton, H.E., Indrayudha, P., Michavila, C., Mukhopadhyay, R., Maurer, S.K., Caulton, S.G., Emsley, J., and Dreveny, I. (2018). The structure of the deubiquitinase USP15 reveals a misaligned catalytic triad and an open ubiquitin-binding channel. J. Biol. Chem. *293*, 17362–17374.

Yan, X., Liu, Z., and Chen, Y. (2009). Regulation of TGF-beta signaling by Smad7. Acta Biochim. Biophys. Sin. *41*, 263–272.

Zhang, L., Zhou, F., Drabsch, Y., Gao, R., Snaar-Jagalska, B.E., Mickanin, C., Huang, H., Sheppard, K.-A., Porter, J.A., Lu, C.X., et al. (2012). USP4 is regulated by AKT phosphorylation and directly deubiquitylates TGF-β type I receptor. Nat. Cell Biol. *14*, 717–726.

Zhang, Q., Harding, R., Hou, F., Dong, A., Walker, J.R., Bteich, J., and Tong, Y. (2016a). Structural basis of the recruitment of ubiquitin-specific protease USP15 by spliceosome recycling factor SART3. J. Biol. Chem. *291*, 17283–17292.

Zhang, W., Wu, K.-P., Sartori, M.A., Kamadurai, H.B., Ordureau, A., Jiang, C., Mercredi, P.Y., Murchie, R., Hu, J., Persaud, A., et al. (2016b). System-wide modulation of HECT E3 ligases with selective ubiquitin variant probes. Mol. Cell *62*, 121–136.

Zhang, W., Sartori, M.A., Makhnevych, T., Federowicz, K.E., Dong, X., Liu, L., Nim, S., Dong, A., Yang, J., Li, Y., et al. (2017). Generation and validation of intracellular ubiquitin variant inhibitors for USP7 and USP10. J. Mol. Biol. *429*, 3546–3560.

Zou, Q., Jin, J., Hu, H., Li, H.S., Romano, S., Xiao, Y., Nakaya, M., Zhou, X., Cheng, X., Yang, P., et al. (2014). USP15 stabilizes MDM2 to mediate cancer-cell survival and inhibit antitumor T cell responses. Nat. Immunol. *15*, 562–570.

Zwart, P.H., Afonine, P.V., Grosse-Kunstleve, R.W., Hung, L.-W., Ioerger, T.R., McCoy, A.J., McKee, E., Moriarty, N.W., Read, R.J., Sacchettini, J.C., et al. (2008). Automated structure solution with the PHENIX suite. Methods Mol. Biol. *426*, 419–435.

STAR★METHODS

KEY RESOURCES TABLE

REAGENT or RESOURCE	SOURCE	IDENTIFIER
Antibodies		
anti-Ub P4D1	Santa Cruz	Cat# sc-8017; RRID: AB_628423
anti-HA Y-11	Santa Cruz	Cat# sc-805; RRID: AB_631618
anti-Myc 9E10	Santa Cruz	Cat# sc-40; RRID: AB_627268
anti-TβR-I V-22	Santa Cruz	Cat# sc-398; RRID: AB_632493
anti-TβR-I R-20	Santa Cruz	Cat# sc-399; RRID: AB_632490
anti-MYC	Sigma	Cat# C3956; RRID: AB_439680
anti-β-actin	Sigma	Cat# A1978; RRID: AB_476692
anti-FLAG	Sigma	Cat# F7425/ F1804; RRID: AB_439687/AB_262044
anti-actin	Millipore	Cat# MAB1501; RRID: AB_2223041
anti-USP15	Abcam	Cat# ab56900/ab97533; RRID: AB_946080/AB_10678830
anti-TRIM25	Proteintech	Cat# 12573-1-AP; RRID: AB_2209732
anti-Xpress	Life Technologies	Cat# R910-25; RRID: AB_2556552
Bacterial and Virus Strains		
Escherichia coli: BL21 (DE3)	NEB	Cat# C2527I
Chemicals, Peptides, and Recombinant Proteins		
USP15 full length	Boston Biochem	Cat# E-594
Ub-AMC	Boston Biochem	Cat# U-550
Ubiquitin-Rhodamine 110	Boston Biochem	Cat# U-555
Critical Commercial Assays		
Simply P Total RNA extraction kit	Bioflux	Cat# BSC52S1
High Capacity cDNA Reverse Transcription kit	Applied Biosystems	Cat# 4368814
Dual luciferase system	Promega	Cat# E1910
Deposited Data		
USP15-DUSP/UbV.15.D structure	This paper	PDB: 6DJ9
USP15-D1D2/UbV.15.2 structure	This paper	PDB: 6CRN
USP15-D1D2/UbV.15.1a structure	This paper	PDB: 6ML1
USP15-D1D2/UbV.15.1d structure	This paper	PDB: 6CPM
Affinity-based mass spectrometry performed with UbVs	This paper; ProteomeXchange Consortium	PXD011840
Experimental Models: Cell Lines		
Human: HEK293T	ATCC	Cat# CRL-3216
Oligonucleotides		
shRNA targeting USP15: 5′-GGAACACCTTATTGATGAA-3′	This paper	N/A
qRT–PCR primers for SMAD7: 5'-AAACAGGGGGAACGA ATTATC-3' and 5'-ACCACGCACCAGTGTGAC-3'	This paper	N/A
qRT–PCR primers for GAPDH: 5′-AACAGCGACACCCAC TCCTC-3′ and 5′-CATACCAGGAAATGAGCTTGAC-3′	This paper	N/A
Recombinant DNA		
pHH0103 GST-TEV-USP15 FLΔinsert (1-471, 780-981)	This paper	N/A
pHH0103 GST-TEV-USP15 CD (275-981)	This paper	N/A
pHH0103 GST-TEV-USP15 D1D2 (275-471,780-981)	This paper	N/A
pHH0103 GST-TEV-USP15 D1D2Δ1 (275-471,780-934)	This paper	N/A

(*Continued on next page*)

Continued

REAGENT or RESOURCE	SOURCE	IDENTIFIER
pHH0103 GST-TEV-USP15 D1D2Δ2 (275-471,863-934)	This paper	N/A
pHH0103 GST-TEV-USP15 DUSP (1-133)	This paper	N/A
pHH0103 GST-TEV-USP15 Ubl1 (128-231)	This paper	N/A
pHH0103 GST-TEV-USP15 Ubl2 (470-559)	This paper	N/A
pGL2-Firefly	Rene Bernards (NKI, Amsterdam)	N/A
pGL2-*Renilla*	Rene Bernards (NKI, Amsterdam)	N/A
pcDNA3-HA-Ub	Addgene	Cat# 18712
pcDNA-Xpress-His-USP15	Addgene	Cat# 23216
pRK-Myc-SMURF2	Addgene	Cat# 13678
pCMV-FLAG-USP15	MRC Unit at the University of Dundee	DU42487
pEF-TRIM25-FLAG	J.U. Jung (University of Southern California)	N/A
Software and Algorithms		
PEAKS software version 8.5	Bioinformatics Solutions Incorporated	N/A
PyMOL	Schrödinger, LLC	http://www.pymol.org/
Discovery Studio	Biovia	https://www.3dsbiovia.com/
PHENIX crystallography suite	Zwart et al. (2008)	https://www.phenix-online.org/
HKL2000	Otwinowski and Minor (1997)	http://www.hkl-xray.com/hkl-3000
PHASER	McCoy et al. (2007)	http://www.phaser.cimr.cam.ac.uk/
MOLPROBITY	Chen et al. (2010)	http://molprobity.biochem.duke.edu/
COOT	Emsley and Cowtan (2004)	http://www2.mrc-lmb.cam.ac.uk/Personal/pemsley/coot/
Prism 8	GraphPad Software	https://www.graphpad.com/
Swiss-Modeller	Biasini et al. (2014)	https://swissmodel.expasy.org/

CONTACT FOR REAGENT AND RESOURCE SHARING

Further information and requests for reagents may be directed to, and will be fulfilled by the Lead Contact Sachdev S. Sidhu (sachdev.sidhu@utoronto.ca).

EXPERIMENTAL MODEL AND SUBJECT DETAILS

Recombinant Proteins

All recombinant proteins used for *in vitro* studies were expressed in E. coli BL21 (DE3) cells (NEB) and they were grown at 37°C in Luria Bertani to an OD600 of 0.6–0.8 and induced with 0.2 mM isopropyl b-D-1-thiogalactopyranoside (IPTG) at 18–20°C overnight.

Cell Culture

For each cell biology experiment, HEK293T cells were transiently transfected with expression plasmids and grown as described in Method Details.

METHOD DETAILS

Library Construction

Phage-displayed libraries were constructed using a phagemid and methods described previously (Ernst et al., 2013). Hard randomization was achieved by using NNK (K = G/T) degenerate codons that contain 32 codons encoding for 20 amino acids, and soft randomization was achieved by allowing 70% of the wild-type base and 10% each of the other three bases at every nucleotide position of mutagenized codons. The libraries were constructed using site-directed mutagenesis by simultaneously targeting two or three regions of Ub with varying combinations of degenerate oligonucleotides (Ernst et al., 2013), and the oligonucleotide design and combinations are described in Table S1. Libraries 4, 4a and 4b contained 2.5 x 10^{10}, 5 x 10^{9} and 3 x 10^{9} unique members, respectively.

Protein Expression and Purification

USP15 and USP4 protein fragments were expressed as fusions to the C-terminus of the hexa-His-tagged glutathione *S*-transferase (GST) using an in-house IPTG-inducible plasmid (pHH0103)(Teyra et al., 2017). PCR amplified DNA fragments encoding the indicated UbVs with an N-terminal FLAG epitope tag were cloned into the Gateway Entry vector pDONR221 (Thermo Fisher) according to the manufacturer's instructions and then transferred into the Gateway Destination expression vector pET53 (His-tagged, Thermo Fisher). *Escherichia coli* BL21 (DE3) (NEB) harboring expression plasmids were grown in 2YT medium supplemented with 100 μg/ml ampicillin with shaking at 200 rpm at 37°C to an OD_{600} ~0.6. Protein expression was induced by addition of IPTG (isopropyl β-D-1-thiogalactopyranoside, Bioshop) at mid-log phase to a final concentration of 1 mM. After incubation overnight at 16°C with shaking, cell pellets were collected by centrifugation (12,200 x g, 10 min) and lysed by sonication, and proteins were purified using nickel-nitrilotriacetic acid (Ni-NTA) Agarose resin (Qiagen 30250) at 4°C following the manufacturer's instructions. The purity of eluted fractions was determined by polyacrylamide gel electrophoresis demonstrating a major band at the expected size. Protein concentrations were determined by measuring the absorption at 280 nm (Nanodrop 2000, Thermo Fisher). Eluted proteins were dialyzed into 50 mM HEPES buffer pH 7.5, 250 mM NaCl, 5% glycerol, 1 mM DTT and stored at 4°C or frozen at -80°C for further applications.

Phage-Displayed UbV Selections

The phage-displayed UbV libraries were independently selected against the different GST-tagged USP15 protein fragments. Phage display selections were performed as described (Ernst et al., 2013), by cycling phage pools through rounds of binding selections with purified USP15 protein fragments immobilized on 96-well Maxisorp plates (Thermo Fisher 12565135). To eliminate phage that bound nonspecifically, input phage pools were first incubated on plates coated with GST (rounds 2–5). After five rounds, phage from individual colonies were assessed for binding to immobilized proteins by phage ELISA (Persson et al., 2013), and clones that bound to target protein but not to negative control proteins were subjected to DNA sequencing to decode the sequence of the displayed UbV (Tonikian et al., 2007).

ELISAs to Evaluate Binding and Specificity

Proteins in study were immobilized on 384-well MaxiSorp plates (Thermo Fisher 12665347) by adding 30 μL of 1 μM proteins for overnight incubation at 4°C. Phage and protein ELISAs against immobilized proteins was performed as described (Ernst et al., 2013). Binding of phage was detected using anti-M13-HRP antibody (GE Healthcare 27942101) and binding of FLAG-tagged UbVs was detected using anti-FLAG-HRP antibody (Sigma-Aldrich A8592). To measure the half maximal binding concentration (EC50) of UbVs binding to the target protein, the concentration of UbVs or Ub.wt was typically varied from 0-1 μM (12 points, 1:2 dilution), while the concentration of target proteins immobilized on the plate remained at 1 μM. EC50 values were calculated using the GraphPad Prism software with the built-in equation formula (dose-response non-linear regression curve). Data were presented as the mean ± SD (n = 3).

Enzyme Activity and Inhibition Assays

USP enzymatic activity and inhibition assays were measured at room temperature using the cleavage-sensitive fluorogenic substrate Ub-AMC (Boston Biochem, U-550) or Ub-Rh110, as described (Ernst et al., 2013). Enzyme activity assays were performed in assay buffer (50 mM PBS pH 7.4, 0.01% Tween 20, 10 mM DTT) containing 0.5 nM USP15 or 25 nM USP4 constructs and serial dilutions of Ub-AMC. The AMC fluorescence emission was monitored at 460 nm (excitation at 360 nm) for 30-60 min using a BioTek Synergy2 plate reader (BioTek Instruments). Duplicates of initial reaction velocity (nM/s) were determined at each substrate concentration by determining the linear slope from plotting fluorescence signal versus time and converting to molarity by interpolating from a standard curve of known AMC concentrations. Typically, the linear accumulation of the product started after the first 100 seconds of the reaction. Velocity versus substrate concentration was plotted to determine the K_M and V_{max} values using GraphPad Prism with the Michaelis–Menten equation, $V_0 = V_{max}*[S]/(K_M + [S])$. The k_{cat} value was obtained from the equation $k_{cat} = V_{max}/[E]_o$, where $[E]_o$ is the total enzyme concentration.

Enzyme inhibition assays were performed in assay buffer containing 1 μM substrate (Ub-Rh110 for full-length and Ub-AMC for fragment proteins), serial dilutions of UbV, and a USP concentration ranging from 0.5 nM to 5 nM depending on how much enzyme was needed to show linear activity in the first 10-15 minutes, except for USP4 CD where 25 nM was required. USP and UbV were mixed in assay buffer and incubated for 10 min before the addition of the substrate. Proteolytic activity was measured for 30 min in duplicates, and the initial reaction velocities (nM/s) were determined for each UbV concentration. Velocity versus UbV concentration was plotted and fitted using the GraphPad Prism software with the built-in equation formula (non-linear regression curve), and the concentration of UbV that inhibits 50% of USP activity (IC_{50}) was determined.

Protein Purification for Crystallization and Structure Determination

For crystallization experiments, a Tobacco Etch Virus (TEV) protease cleavage site was introduced between the 6x His-FLAG and the UbV in the pET53-UbV plasmid, and between the His-GST and the USP15 construct in the pHH0103-USP15 plasmid. Competent *Escherichia coli* BL21 (DE3) cells (NEB) were transformed and grown in a 1 L culture, cells were lysed by sonication and clarified by centrifugation in a manner similar to that described above. Proteins were purified on Ni-NTA resin, protein tags were cleaved by overnight dialysis with in-house TEV protease 1:30 (wt/wt) into PBS at 4°C, and re-purified on Ni-NTA resin to remove His-tagged TEV protease and other impurities. Resulting flow-through containing the USP15 fragment and UbV of interest were mixed and

concentrated to approximately 10 mg/ml. UbV concentration was always higher than USP15 and the excess UbV was removed by gel filtration on a Superdex 75 16/600 GL column (GE Healthcare) equilibrated in a buffer containing 20 mM HEPES, pH 7.5, 150 mM NaCl and 1 mM DTT. Fractions corresponding to the USP15/UbV complex, as determined from SDS-PAGE, were pooled together, concentrated to 10-25 mg/ml and exchanged into a buffer containing 20 mM HEPES, pH 7.5, 50 mM NaCl, and 1 mM DTT using Amicon Ultra-4 filters (Millipore; UFC810024), flash-frozen in 100 μl aliquots in liquid Nitrogen, and stored at -80°C. Protein concentrations were determined by measuring UV absorbance at 280 nm using NanoDrop 2000 (Thermo Fisher).

Initial crystallization trials for USP15 D1D2Δ1 bound to UbV.15.2 and USP15 DUSP bound to UbV.15.D were performed using the Mosquito LCP crystallization robot (TTP Labtech) using a number of commercial 96-well screens such as JCSG-Plus (Molecular Dimensions), ProPlex HT-96 (Molecular Dimensions), PACT Premiere (Molecular Dimensions), SaltRX (Hampton Research) and Protein Complex (Qiagen). The USP15 D1D2Δ1/UbV.15.2 complex (23 mg/ml) was crystallized in a liquor containing 25% PEG3350, 200 mM Potassium Citrate tribasic and 100 mM MES pH 6.5. The USP15 D1D2Δ2/UbV.15.1a complex (9 mg/ml) was crystallized in a liquor containing 16% PEG3350, 150 mM $CaCl_2$ and 100 mM MES 6.5. The USP15 D1D2Δ2/UbV.15.1d complex (12.8 mg/ml) was crystallized in the identical buffer as 15.1a except containing 150 mM $CaCl_2$. The USP15 DUSP/UbV.15.D complex was crystallized in 16% PEG6K, 100 mM Sodium Citrate pH 5.0 and 100 mM Magnesium Chloride. Prior to data collection, drops containing these crystals were equilibrated in equivalent crystallization liquor containing either 25-30% glycerol or ethylene glycol, and then crystals were individually harvested and flash-frozen in liquid nitrogen.

Diffraction data were collected at beamline 24-ID-C or 24-ID-E (NE-CAT) at Argonne National Laboratories (Chicago), except for a single crystal of USP15 D1D2Δ2/UbV.15.1d that was collected on an in-house X-ray diffractometer (Rigaku MicroMax 007 diffractometer, l=1.54 A, Rigaku RAXIS++ detector). All datasets were processed with either HKL2000 (Otwinowski and Minor, 1997) or MOSFLM (Battye et al., 2011), and were solved by molecular replacement using Phenix.Phaser (McCoy et al., 2007) within the PHENIX crystallography suite (Zwart et al., 2008), and subsequent model refinement and water picking was performed either automatically with Phenix.refine within the PHENIX crystallography suite or manually using the graphics program Coot (Emsley and Cowtan, 2004). In addition, TLS parameters were generated from the complex coordinates and used during refinement (Urzhumtsev et al., 2013). For the USP15 D1D2Δ1/UbV.15.2 complex, coordinates for the USP4 D1D2 domain structure (PDB entry: 2Y6E) and a model of UbV.15.2 generated with Swiss-Modeller (Biasini et al., 2014) were used as search models. For subsequent structures the USP15 D1D2Δ1 and UbV.15.2 coordinates from this structure were used as search models. For the DUSP/UbV.15.D complex, appropriate coordinates from a USP15 DUSP-Ubl-1 structure (PDB entry: 4A3O) and a Swiss-Model of UbV.15.D were used as search models. For the USP15 DUSP/UbV.15.D complex structure, refinement with corrections for tNCS and for the twinning operator (k,h,-l) were used in Phenix.refine, in which the crystal was treated as virtually merohedrally twinned (twinning fraction of 0.49).

The final models were validated using MOLPROBITY (Chen et al., 2010). All final structures showed good geometry; virtually no Ramachandran outliers and a good clash score (Table 2). However, general conformational mobility for the UbV was observed for the final refined models of the USP15/UbV structures, as observed by higher B-factors, weaker density and a significantly higher ratio of RSRZ outliers. The USP15 catalytic domains showed poor electron density in the loop containing the catalytic cysteine, and for USP15 D1D2 in complex with UbV.15.1a, the density for this cysteine residue and its neighbors was not modeled. This observation agrees with the free structure of USP15 D1D2 (PDB ID: 6GHA), where the loop was modeled but with elevated B-factors that were associated with conformational mobility (Ward et al., 2018). The structure of USP15 D1D2Δ1 in complex with UbV.15.1a also showed additional density in one of the two USP15/UbV heterodimers in the asymmetric unit that was not present in the UbV.15.1d or UbV.15.2 structures. This density could only be explained by a few residues from the Ubv N-terminal 6-His tag (chain G in the PDB), and it is not clear whether this tag arose from incomplete cleavage with TEV during preparation of the UbV or retention of the N-terminal TEV-cleaved tag during purification and preparation of the complex.

Plasmids for Mammalian Cell Experiments

For transient intracellular expression, genes encoding for FLAG-tagged UbVs were cloned into pcDNA3.1/nFLAG destination plasmid using Gateway Technology (Invitrogen). The pcDNA3.1/nFLAG vector was obtained from the SPARC Biocentre (Hospital for Sick Children, Toronto, Canada), and the pGL2-Firefly and pGL2-*Renilla* luciferase reporter vectors were gifts from Rene Bernards (NKI, Amsterdam, Netherlands). Expression plasmids pcDNA3-HA-Ub, pcDNA-Xpress-His-USP15 and pRK-Myc-SMURF2 were purchased from Addgene (plasmid IDs: 18712, 23216 and 13678, respectively), pCMV-FLAG-USP15 was purchased from the MRC unit at the University of Dundee (DU42487), and pEF-TRIM25-FLAG plasmid was provided by J.U. Jung (Harvard Medical School, University of Southern California Keck School of Medicine). Xpress-USP15 was used as a template to produce C269A mutant by site-directed mutagenesis. The constitutively active TβR-I (TRICA) vector was a kind gift from Joan Seoane. The shRNA sequence targeting USP15 (5′-GGAACACCTTATTGATGAA-3′) was cloned into pRetroSuper plasmid, and the shRNA targeting the mouse-specific B subunit (PR59) used as a negative control was cloned into pRS plasmid.

Immunoprecipitation and Mass Spectrometry

For affinity purification coupled with mass spectrometry, HEK293T cells were transiently transfected with expression plasmids containing FLAG-tagged UbVs, lysed in high salt buffer, subjected to immune-affinity purification using immobilized anti-FLAG M2 affinity agarose beads (Sigma-Aldrich A2220), and digested with TPCK-trypsin (Thermo Fisher 20233), as described (Marcon et al., 2015). The tryptic peptide samples were analyzed by liquid chromatography-tandem mass spectrometry (LC-MS/MS) on

an Orbitrap analyzer (Q-Exactive, Thermo Fisher), as described (Tong et al., 2017). Raw files acquired from the mass spectrometer were processed using PEAKS software version 8.5 (Bioinformatics Solutions Incorporated) against the Uniprot Human Database modified to include the UbV bait sequences. Label-free quantification (LFQ) values of each protein were exported from PEAKS and a peptide between the FLAG-tag and the UbV (K.GQGPDPSTNSADITSLYK.K), which is common to all UbV proteins, was used for the normalization of USP15 and USP4 expression.

Luciferase-Based TGF-β Reporter Assay

Luciferase assays were performed using the Dual luciferase system (Promega). HEK293T cells were transiently co-transfected with a combination of plasmids encoding CAGA-Firefly luciferase (1.5 μg), *Renilla* luciferase (0.3 μg) and either USP15-shRNA (5 μg), FLAG-tagged USP15 (1 μg), FLAG-tagged UbV.15.1a (1 μg), FLAG-tagged diUbV.15.1/D (1 μg), or a negative control vector [pRS-PR59 (5 μg) for USP15-shRNA or pcDNA3.1/nFLAG (1 μg) for all UbV expression constructs]. Transfection was performed using the calcium phosphate method as described (Kit Leng Lui et al., 2017). In short, DNA was resuspended in 1.5 ml HEPES buffered saline/calcium chloride solution. Resultant reagent mix was spread amongst 6 wells of a 12 well plate with 200 μl added to each well. After 48 hours (or 72 hours for USP15-shRNA), 100 pM TGF-β was added overnight in the presence of DMEM (0% FCS) and cells were lysed the next day (approximately 16 hours of stimulation). Luciferase counts were measured using a Sirius Luminometer (Berthold), and after normalizing the firefly luciferase activity to Renilla luciferase activity, an unpaired two-tailed Student's t test was performed to calculate the p values. Activities were measured in triplicate and assays were repeated independently at least three times.

Quantitative Real-Time PCR (qRT-PCR)

HEK293T cells were transiently transfected with a pcDNA3.1/nFLAG empty vector or a vector expressing diUbV.15.1/D. After 48 hours, the cells were treated with TGF-β (2.5 ng/ml) for 3 hours, collected and washed twice in PBS, and RNA was isolated using Simply P Total RNA extraction kit (Bioflux BSC52S1). RNA (2 μg) was reverse transcribed using the High Capacity cDNA Reverse Transcription kit (Applied Biosystems 4368814). PCR data were captured using ABI 7900 or 7500 FAST sequence detector (Perkin Elmer). The qRT–PCR primers used for SMAD7 were 5'-AAACAGGGGGAACGAATTATC-3' and 5'-ACCACGCACCAGTGTGAC-3', and for GAPDH were 5′-AACAGCGACACCCACTCCTC-3′ and 5′-CATACCAGGAAATGAGCTTGAC-3′. GAPDH mRNA was used as an internal normalization control and relative mRNA values between SMAD7 and GAPDH were calculated using the ΔΔCt method (Livak and Schmittgen, 2001).

Immunoprecipitation and In Vivo Deubiquitination Assays

For the SMURF2 deubiquitination assays, HEK293T cells were transiently co-transfected with expression plasmids containing Myc-tagged SMURF2, HA-Ub and FLAG-tagged diUbV.15.1/D or pcDNA3.1/nFLAG empty vector at a 1:1 ratio. Cells were treated with the proteasome inhibitor MG132 (5 μM, Sigma M7449) for 16 hours before collection, and lysed after 48 hours in ELB buffer. For the TRIM25 deubiquitination assays, HEK293T cells were transiently co-transfected with expression plasmids containing FLAG-tagged TRIM25, either Xpress-tagged USP15 wild-type or C269A point mutant, with or without FLAG-tagged UbVs (15.1a and 15.1/D) at a 1:1 ratio. Cells were lysed after 24 hours in RIPA buffer.

After centrifugation to remove insoluble material, an aliquot of lysate was added to sample buffer (whole cell lysate, WCL) and the remaining lysate was incubated overnight with 5 μg of the indicated antibodies, and then added protein G Sepharose beads (Invitrogen) for 2 hours at 4 degrees. Immunoprecipitated and WCL samples were separated by 10% and 15% SDS-PAGE and transferred to polyvinylidene difluoride membranes (Millipore). Membranes were blocked with bovine serum albumin or 5% milk. Blots were probed with specific antibodies as indicated, incubated with HRP-linked secondary antibody, and resolved with chemiluminescence (Pierce 32106/Thermo Fisher 34080). The following antibodies were used: anti-Ub P4D1 (sc-8017), anti-HA Y-11 (sc-805), anti-Myc 9E10 (sc-40), and anti-TβR-I V-22 (sc-398)/R-20 (sc-399) from Santa Cruz; anti-MYC (C3956), anti-β-actin (A1978), and anti-FLAG (F7425/ F1804) from Sigma; anti-β-actin (MAB1501) from Millipore; anti-USP15 (ab56900/ab97533) from Abcam; anti-TRIM25 (12573-1-AP) from Proteintech; anti-Xpress (R910-25) from Life Technologies.

DATA AND SOFTWARE AVAILABILITY

The atomic coordinates for USP15-DUSP/UbV.15.D, USP15-D1D2/UbV.15.2, USP15-D1D2/UbV.15.1a and USP15-D1D2/UbV.15.1d complexes reported in this paper are deposited to the Protein Data Bank under PDB accession codes 6DJ9, 6CRN , 6ML1 and 6CPM, respectively. The mass spectrometry results for the co-immunoprecipitation assays with the UbVs have been deposited to the ProteomeXchange via the PRIDE partner repository (Vizcaíno et al., 2014) with identifier PXD011840.

Structure, Volume *27*

Supplemental Information

Structural and Functional Characterization of Ubiquitin Variant Inhibitors of USP15

Joan Teyra, Alex U. Singer, Frank W. Schmitges, Patrick Jaynes, Sarah Kit Leng Lui, Maria J. Polyak, Nassima Fodil, Jonathan R. Krieger, Jiefei Tong, Carsten Schwerdtfeger, Bradley B. Brasher, Derek F.J. Ceccarelli, Jason Moffat, Frank Sicheri, Michael F. Moran, Philippe Gros, Pieter J.A. Eichhorn, Martin Lenter, Guido Boehmelt, and Sachdev S. Sidhu

Supplementary Figures and Tables:

Figure S1. Related to Figure 1: Activity assays for USP15 and USP4.

(A) Ub-AMC substrate dose response activity curves for various USP15 protein fragments fitted to the Michaelis-Menten equation. **(B)** Activity curves for a fixed concentration of USP15 protein incubated with 2-fold serial dilutions of Ub-AMC substrate in duplicates (10-0.005 µM). Changes of AMC fluorescence emission at 460 nm (excitation at 360 nm) were monitored and the linear parts of the data were used to calculate initial velocities. **(C)** Ub-AMC substrate dose response activity curves for USP4 CD fitted to the Michaelis-Menten equation. **(D)** Activity curves for a fixed concentration of USP4 CD protein incubated with 2-fold serial dilutions of Ub-AMC substrate in duplicates (10-0.005 µM). Changes of AMC fluorescence emission at 460 nm (excitation at 360 nm) were monitored and the linear parts of the data were used to calculate initial velocities.

Figure S2. Related to Figure 2: ELISAs for UbVs binding to USP15 and USP4 protein fragments

UbV binding curves to USP15 and USP4 protein fragments were measured by ELISA. The half maximal effective binding concentration (EC_{50}) was defined as the UbV concentration required to achieve half of the saturating binding signal.

Figure S3. Related to Figure 2: ELISAs for UbVs binding to USP15 protein fragments

(A,B) ELISA curves for UbVs binding to **(A)** USP15 FLΔInsert or **(B)** USP15 D1D2. **(C)** The half maximal effective binding concentration (EC_{50}) was defined as the UbV concentration required to achieve half of the saturating binding signal. **(D,E)** ELISA curves for UbVs binding to **(D)** USP15 FLΔInsert, **(E)** USP15 D1D2 and negative controls (GST and BSA).

Figure S4. Related to Table 1: Inhibition of USP15 FLΔinsert activity by UbVs.

Dose response curves for the inhibition of Ub-AMC hydrolysis by **(A)** USP15 FLΔinsert with UbVs selected for binding to the USP15 modular domains, and by **(B)** USP15 FLΔinsert, **(C)** USP15 CD and **(D)** USP4 CD with UbVs selected for binding to the USP15 catalytic domain. The IC_{50} values were determined as the concentration of UbV that reduced proteolytic activity by 50% and are show in **Table 1**.

Figure S5. Related to Figure 5 and 6: Size exclusion chromatography of UbV/USP15 complexes

Representative gel filtration traces using HiLoad™ 16/600 Superdex™ 75 pg (GE Healthcare) are shown at the top for mixtures of UbV.15.D and USP15 DUSP domain (orange) or UbV.15.2 and USP15 D1D2 (blue), and SDS-PAGE of the indicated peak fractions are shown at the bottom. UbV proteins were added in excess to enable visualization of both free UbV and UbV in complex with USP15 protein. Elution time (ml) is inversely proportional to molecular weight (Mwt), which is calculated for each protein sequence using the ProtParam server (http://web.expasy.org/protparam/)

Figure S6. Related to Figure 5: Comparative analysis of the DUSP/UbV.15.D complex structure.

A) Superposition of a single subunit of UbV.15.D (orange) with Ub.wt (grey; PDB Id 1UBQ), where β1' strand from UbV.15.D' subunit is treated as β1 (red). B) Superposition of the strand-exchange dimers of UbV 15.D (green) and UbV.XR$_D$ (red; PDB Id 5OST) taking one of the UbV subunits as a reference and calculating the relative orientation of the other subunit. C) Sequence alignment of Ub.wt, UbV.XR.D and UbV.15.D, and amino acid differences relative to Ub.wt are highlighted in red. D) Front (left) and lateral (right) perspectives of the USP15 DUSP/UbV.15.D (top) and XIAP/UbV.XR.D (bottom) complexes. UbV subunits are represented as red and pink ribbons, and the DUSP and XIAP domains are represented as green and yellow ribbons. E) Superposition of the structures of the DUSP domains of USP15 (red) and USP4 (cyan; PDB entry: 5CTR). F) Superposition of the structure of the DUSP domain of USP15 (red) bound to UbV.15.D dimer (green) with the structure (PDB entry: 5JJW) of the DUSP domain of USP15 (orange) bound to the SART3 HAT domain (yellow). Superposition was performed for the DUSP domains only. The interface of the DUSP domain with UbV.15.D or the SART3 HAT domain is demarcated by a closed or dashed circle, respectively.

Figure S1:

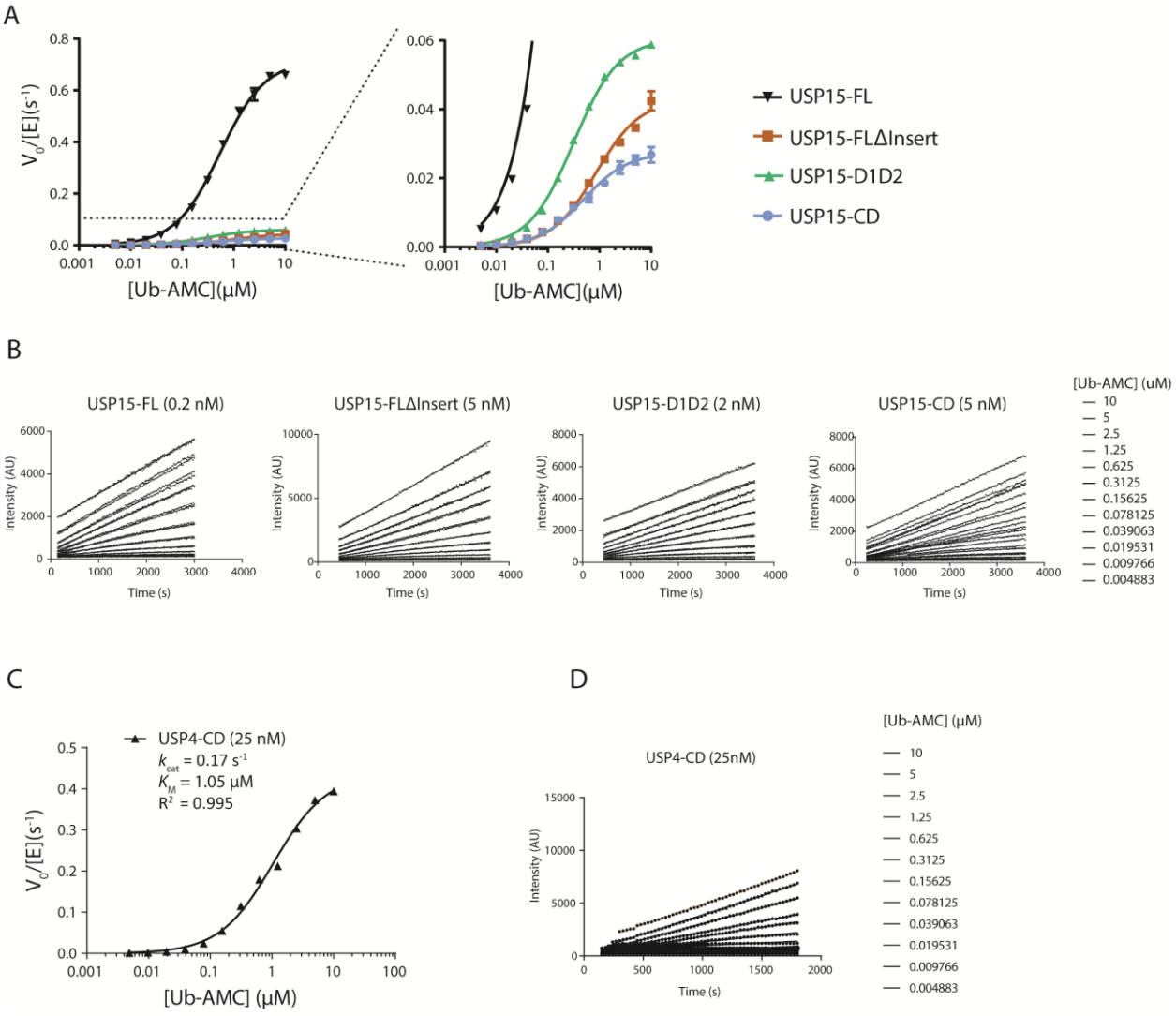
A
$V_0/[E](s^{-1})$
[Ub-AMC](μM)
USP15-FL
USP15-FLΔInsert
USP15-D1D2
USP15-CD
B
USP15-FL (0.2 nM)
USP15-FLΔInsert (5 nM)
USP15-D1D2 (2 nM)
USP15-CD (5 nM)
Intensity (AU)
Time (s)
[Ub-AMC] (uM)
10
5
2.5
1.25
0.625
0.3125
0.15625
0.078125
0.039063
0.019531
0.009766
0.004883
C
USP4-CD (25 nM)
k_{cat} = 0.17 s^{-1}
K_M = 1.05 μM
R^2 = 0.995
$V_0/[E](s^{-1})$
[Ub-AMC] (μM)
D
USP4-CD (25nM)
Intensity (AU)
Time (s)
[Ub-AMC] (μM)
10
5
2.5
1.25
0.625
0.3125
0.15625
0.078125
0.039063
0.019531
0.009766
0.004883

Figure S2:

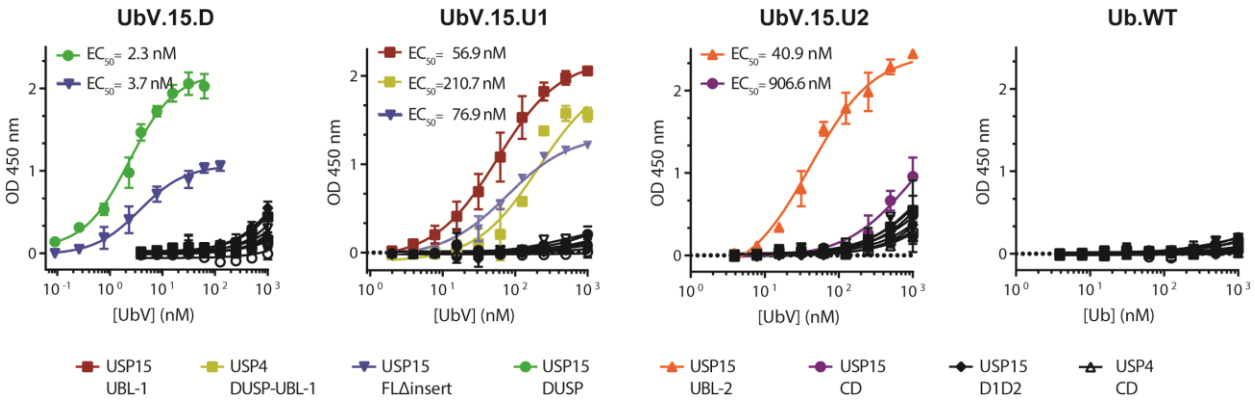
UbV.15.D
EC50= 2.3 nM
EC50= 3.7 nM
OD 450 nm
[UbV] (nM)
UbV.15.U1
EC50= 56.9 nM
EC50=210.7 nM
EC50= 76.9 nM
OD 450 nm
[UbV] (nM)
UbV.15.U2
EC50= 40.9 nM
EC50= 906.6 nM
OD 450 nm
[UbV] (nM)
Ub.WT
OD 450 nm
[Ub] (nM)
USP15 UBL-1
USP4 DUSP-UBL-1
USP15 FLΔinsert
USP15 DUSP
USP15 UBL-2
USP15 CD
USP15 D1D2
USP4 CD

Figure S3:

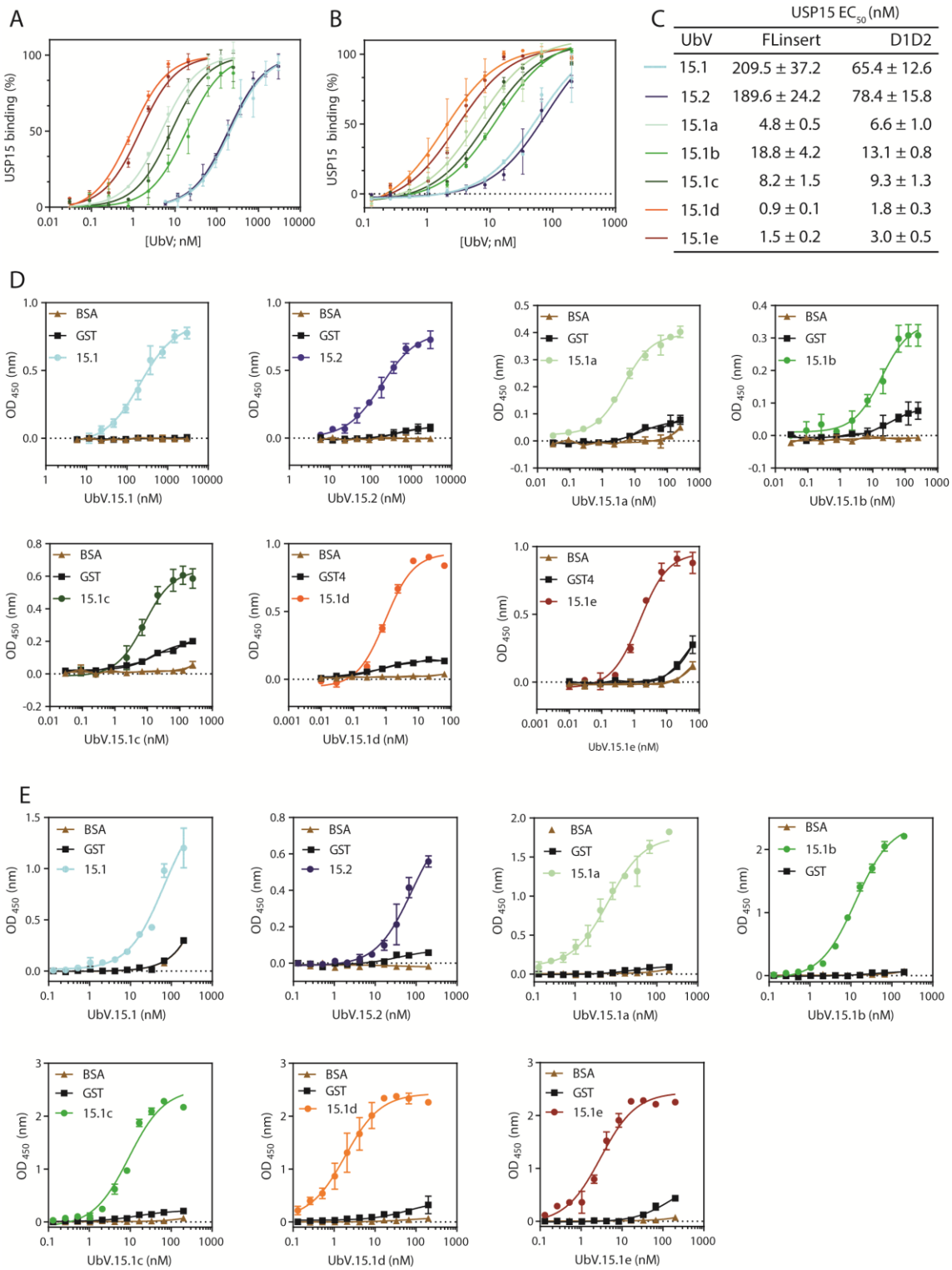
A
B
C
USP15 EC50 (nM)
UbV FLinsert D1D2
15.1 209.5 ± 37.2 65.4 ± 12.6
15.2 189.6 ± 24.2 78.4 ± 15.8
15.1a 4.8 ± 0.5 6.6 ± 1.0
15.1b 18.8 ± 4.2 13.1 ± 0.8
15.1c 8.2 ± 1.5 9.3 ± 1.3
15.1d 0.9 ± 0.1 1.8 ± 0.3
15.1e 1.5 ± 0.2 3.0 ± 0.5
USP15 binding (%)
[UbV; nM]
D
E
BSA
GST
GST4
OD450 (nm)
UbV.15.1 (nM)
UbV.15.2 (nM)
UbV.15.1a (nM)
UbV.15.1b (nM)
UbV.15.1c (nM)
UbV.15.1d (nM)
UbV.15.1e (nM)

Figure S4:

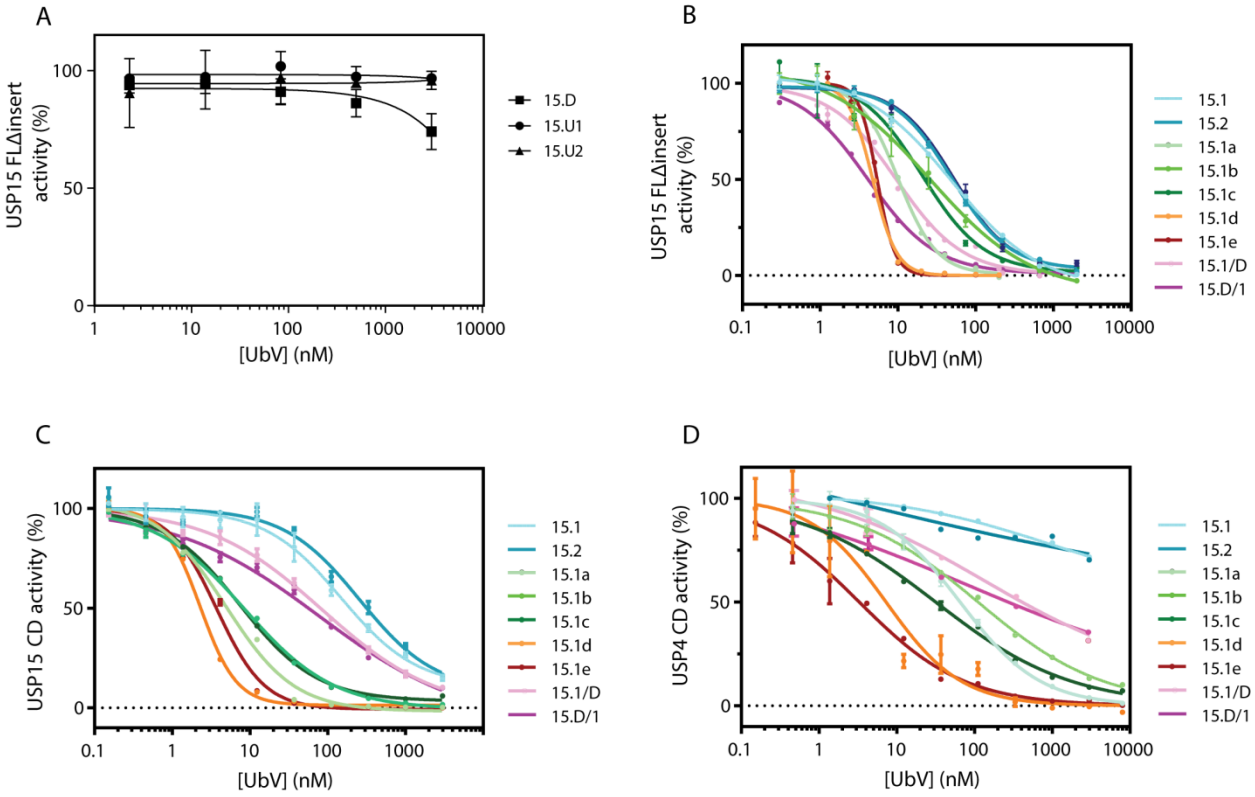
A
USP15 FLΔinsert activity (%)
100
50
0
1
10
100
1000
10000
[UbV] (nM)
15.D
15.U1
15.U2
B
USP15 FLΔinsert activity (%)
100
50
0
0.1
1
10
100
1000
10000
[UbV] (nM)
15.1
15.2
15.1a
15.1b
15.1c
15.1d
15.1e
15.1/D
15.D/1
C
USP15 CD activity (%)
100
50
0
0.1
1
10
100
1000
[UbV] (nM)
15.1
15.2
15.1a
15.1b
15.1c
15.1d
15.1e
15.1/D
15.D/1
D
USP4 CD activity (%)
100
50
0
0.1
1
10
100
1000
10000
[UbV] (nM)
15.1
15.2
15.1a
15.1b
15.1c
15.1d
15.1e
15.1/D
15.D/1

Figure S5:

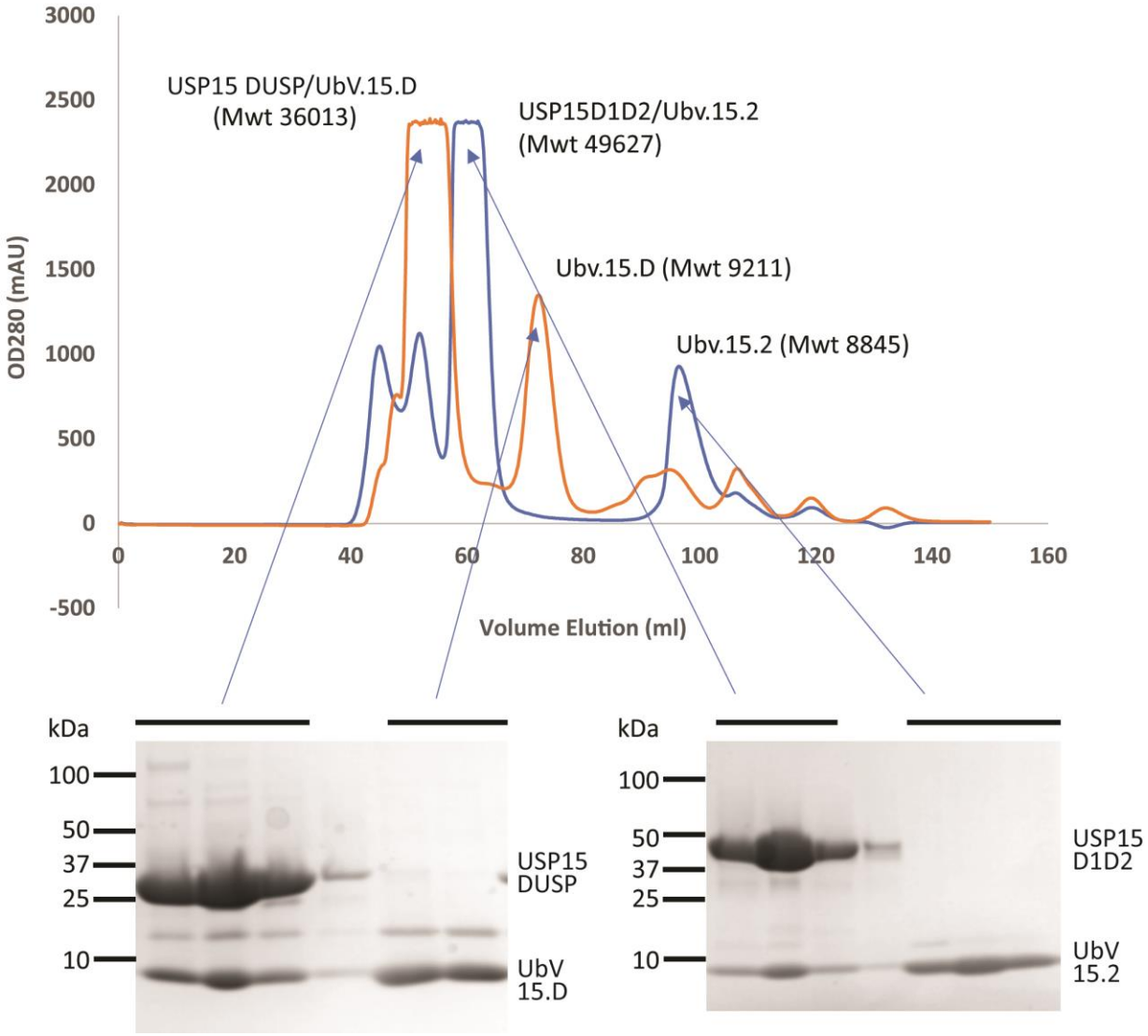
3000
2500
2000
1500
1000
500
0
-500
OD280 (mAU)
0
20
40
60
80
100
120
140
160
Volume Elution (ml)
USP15 DUSP/UbV.15.D
(Mwt 36013)
USP15D1D2/Ubv.15.2
(Mwt 49627)
Ubv.15.D (Mwt 9211)
Ubv.15.2 (Mwt 8845)
kDa
100
50
37
25
10
USP15
DUSP
UbV
15.D
kDa
100
50
37
25
10
USP15
D1D2
UbV
15.2

Figure S6:

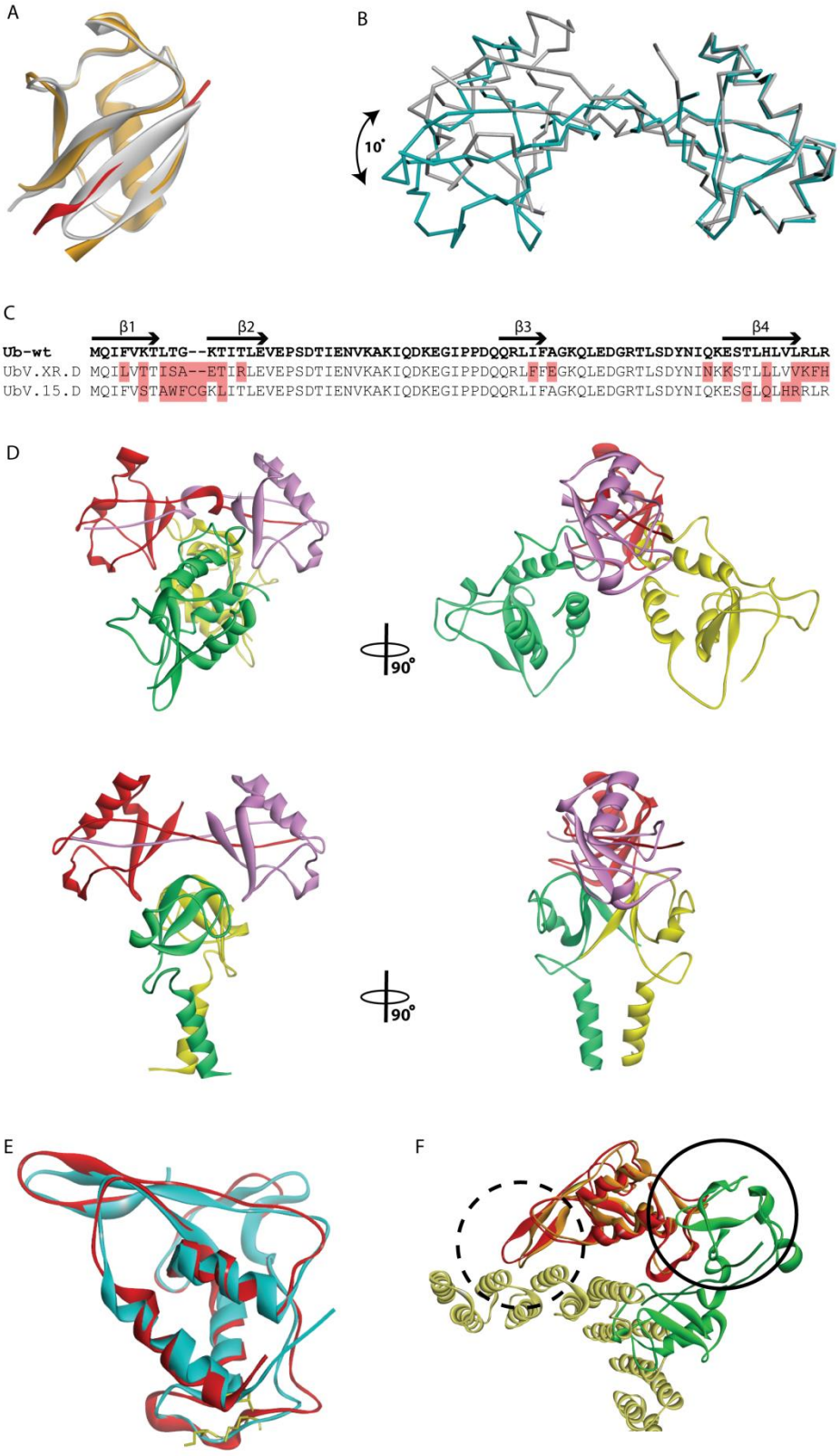
A
B
10°
C
β1
β2
β3
β4
Ub-wt MQIFVKTLTG--KTITLEVEPSDTIENVKAKIQDKEGIPPDQQRLIFAGKQLEDGRTLSDYNIQKESTLHLVLRLR
UbV.XR.D MQILVTTISA--ETIRLEVEPSDTIENVKAKIQDKEGIPPDQQRLFFEGKQLEDGRTLSDYNINKKSTLLLVVKFH
UbV.15.D MQIFVSTAWFCGKLITLEVEPSDTIENVKAKIQDKEGIPPDQQRLIFAGKQLEDGRTLSDYNIQKESGLQLHRRLR
D
90°
90°
E
F

Table S1. Related to Figure 2: Oligonucleotides used for construction of Ubv Libraries

Oligo	Library	Sequence (*)
4.R1.1	4	GAC AAA ATG CAG ATT TTC GTG NNK ACC NNK NNK NNK GGG AAG NNK ATC ACC CTC GAG GTT GAA CCC
4.R1.2	4	GAC AAA ATG CAG ATT TTC GTG NNK ACC NNK NNK NNK NNK GGG AAG NNK ATC ACC CTC GAG GTT GAA CCC
4.R1.3	4	GAC AAA ATG CAG ATT TTC GTG NNK ACC NNK NNK NNK NNK NNK GGG AAG NNK ATC ACC CTC GAG GTT GAA CCC
4ab.R1	4a+4b	GAC GAT GAC AAA ATG (6)(8)(5) ATT (8)(8)(6) GTG (5)(5)(5) (5)(6)(6) (7)(6)(8) (6)(6)(7) (7)(7)(7) (5)(5)(7) (5)(8)(6) ATC (5)(5)(6) CTC GAG GTT GAA CCC
4a.R2	4a	CCT CCT GAT CAG CAG (5)(5)(5) CTG (5)(6)(6) TTT (7)(6)(8) (5)(7)(6) (5)(5)(7) (5)(5)(6) CTG GAA GAT GGA CGT
4b.R2.1	4b	G CAG AGA CTG ATC TTT NNK NNK NNK NNK AAG CAG CTG GAA GAT G
4b.R2.1	4b	G CAG AGA CTG ATC TTT NNK NNK NNK NNK NNK NNK AAG CAG CTG GAA GAT G
4b.R2.1	4b	G CAG AGA CTG ATC TTT NNK NNK NNK NNK NNK NNK NNK NNK AAG CAG CTG GAA GAT G
4.R3	4	C AAT ATT CAA AAG GAG TCT NNK CTT NNK CTT NNK NNK AGA CTT CGT NNK NNK GGC GGT GGC GGA TCC
4ab.R3	4a+4b	G TCT GAC TAC AAT ATT (6)(5)(5) (5)(5)(7) (6)(5)(6) TCT (8)(5)(8) CTT (6)(5)(8) CTT (7)(8)(6) (8)(8)(5) (5)(8)(5) (6)(8)(6) (6)(7)(8) (7)(7)(8) (6)(8)(8) (5)(5)(8) (8)(7)(7) GGC GGA TCC GGT GGC CTC

(*) Numbers denote nucleotide mixtures of 70% of wt nucleotide represented by 5 = A, 6 = C, 7 = G and 8 = T and 10% of each of the other three nucleotides. “N” denotes an equimolar mixture of all four nucleotides. “K” denotes an equimolar mixture of G and T.